Scattering fidelity in chaotic microwave billiards

Dissertation

zur Erlangung des

Doktorgrades der Naturwissenschaften
(Dr. rer. nat.)

dem Fachbereich Physik der

vorgelegt von

Bernd Johann Köber
aus Hermannstadt

Marburg(Lahn), Dezember 2011

Vom Fachbereich Physik der Philipps-Universität Marburg (Hochschulkennziffer: 1180)
als Dissertation angenommen am 17.01.2012

Erstgutachter:	Prof. Dr. H.-J. Stöckmann
Zweitgutachter:	Prof. Dr. P. Lenz
Tag der mündlichen Prüfung:	20.01.2012

Zusammenfassung

Im Rahmen dieser Arbeit wurde mit Hilfe von Mikrowellenexperimenten die zeitabhängige Stabilität von Quantensystemen gegen Störungen untersucht. Für flache Mikrowellen-Resonatoren ist die zugehörige Wellengleichung äquivalent zur Schrödingergleichung, deshalb eignen sich Messungen an so genannten Mikrowellenbillards um quantenmechanische Fragestellungen experimentell zu untersuchen. Um in Quantensystemen die Stabilität der Zeitentwicklung gegen Störungen zu quantifizieren hat Peres [per84] das Überlappintegral der Zeitentwicklung des gleichen Anfangszustands unter einem ungestörten und einem gestörten Hamiltonian eingeführt. Diese Größe nennt man Fidelity oder Loschmidt Echo; sie lässt sich in Mikrowellenbillards unter Verwendung der Scattering Fidelity [sch05a], die sich für chaotische Systeme und schwache Kopplung der Messantennen der gewöhnliche Fidelity annähert, bestimmen.

Im ersten Teil dieser Arbeit werden Untersuchungen des Fidelity-Abfalls in einem klassisch chaotischen Mikrowellenbillard, das durch einen Stempel lokal am Rand deformiert (gestört) werden kann, vorgestellt. Ein vorhergesagter, nicht monotoner Übergang des Loschmidt Echos vom Fermi-Golden-Rule- zum Escape-Rate-Regime [gou08], der mit der Vergrößerung der lokalen Störung des Randes einhergeht, wurde experimentell bestätigt. Des weiteren wurden im Experiment deutliche Oszillationen der Abfallrate in Abhängigkeit der Stempelposition gefunden, die quantitativ mit den zugehörigen theoretischen Ergebnissen aus semiklassischen Beschreibungen zu lokalen Randstörungen übereinstimmen. Die wichtigsten Ergebnisse dieses Abschnitts der Arbeit wurden bereits in [koeb11] veröffentlicht.

Im zweiten Teil dieser Arbeit wurde der Abfall der Fidelity in einem Mikrowellen-Resonator, bei dem die Kopplung variiert wurde, untersucht. Die als Kopplungsfidelity bezeichnete Größe wurde experimentell zunächst für einen angeflanschten Wellenleiter mit variabler Spaltöffnung untersucht. Dabei zeigt sich der Effekt auf die Fidelity durch die Variation der Randbedingung als größer als der Effekt durch die Änderung der Kopplung. Deshalb wurde anstatt des Kanals ein Billard mit einer eingebrachten Antennen mit drei verschiedenen Abschlüssen untersucht. Zum einen wurde die Antenne mit einer Reflexion am festen und offenen Ende und mit einem $50\,\Omega$ Abschluss versehen. Eine quantitative Übereinstimmung mit der theoretischen Beschreibung, die auf einer modifizierten Verbaarschot, Weidenmüller, Zirnbauer (VWZ) Theorie [ver85] beruht, wurde gefunden. Die wichtigsten Ergebnisse dieses Teils, sowie eine detaillierte Beschreibung des Modells in Form eines effektiven Hamiltonian mit komplexer Kopplungskonstanten, entwickelt von D.Savin, wurde in [koeb10] veröffentlicht.

Abstract

In this work microwave experiments are used to study the time dependent stability of quantum systems against perturbations. For flat microwave cavities the corresponding wave equation is equivalent to the Schrödinger equation, therefore measurements with so called microwave billiards are suitable for studying quantum-mechanical questions experimentally. To quantify the stability of quantum time evolution against perturbations Peres [per84] introduced the overlap of the time-evolution of the same initial state under an unperturbed and a perturbed Hamiltonian. This quantity is known as fidelity or Loschmidt echo; it can be determined in microwave billiards using the concept of scattering fidelity [sch05a], which for chaotic systems and weak coupling of the measuring antenna approaches the ordinary fidelity.

In the first part of this work a study of the fidelity decay in classically chaotic microwave billiard for a local, pistonlike boundary perturbation is presented. Experimentally a predicted nonmonotonic crossover from the Fermi golden rule to the escape-rate regime of the Loschmidt echo decay with increasing local boundary perturbation [gou08] is verified. In particular, pronounced oscillations of the decay rate as a function of the piston position have been observed in the experiments which quantitatively agree with corresponding theoretical results based on a refined semiclassical approach for local boundary perturbations. The main results presented in this part have been published in [koeb11].

In the second part of this work the scattering fidelity decay in a microwave billiard is studied for a perturbation, where the coupling to the outside is varied. The resulting quantity, coupling fidelity, is experimentally studied first for an attached wave guide with variable opening of a slit. Thereby the effect on the fidelity due to the change of boundary condition was larger than the effect of the change of coupling. Thus instead of using a channel for the coupling an antenna was introduced and three different terminations attached. Terminations of reflexion on open and closed end and an $50\,\Omega$ load were compared. Quantitative agreement is found with the theory, which is obtained from a modified Verbaarschot, Weidenmüller, Zirnbauer (VWZ) approach [ver85]. The main results presented in this part and a more detailed model description in terms of an effective Hamiltonian with a complex coupling constant developed by D.Savin have been published in [koeb10].

Contents

1 Introduction

The word chaos originally comes from the Greek $\chi\acute{\alpha}o\varsigma$, it refers to the formless or void state preceding the creation of the universe or cosmos in the Greek creation myths, more specifically the initial "gap" created by the original separation of heaven and earth. Nowadays we are used to an informal meaning of chaos as a state of confusion. In mathematics and natural science chaos refers to a very specific kind of unpredictable deterministic behaviour that is very sensitive to its initial conditions.

In 1892 Jules Henri Poincaré published 'Les Méthodes nouvelles de la Mécanique Célesté' [poi92]. In this research on the three-body problem using Isaac Newton's laws of motion (Classical Mechanics) he became the first person to discover a chaotic deterministic system. In his later book 'Science et Méthode'[poi08] he describes such a system as follows:

> Une petite erreur sur les premières produirait une erreur énorme sur les derniers. La prédiction devient impossible et nous avons le phénomène fortuit.

which he illustrates with meteorology, an important field of studying time evolution in physics till this day. At the same time two other fundamental theories, namely quantum mechanics and the theory of relativity started their rapid development. Many physicists were focused on these two theories, so the results of Poincaré lead a shadowy existence until the second half of the last century. Chaos theory was formalized only after the mid-century, when it first became evident for some scientists that linear theory, the prevailing system theory at that time, simply could not explain the observed behaviour of certain experiments (for example a double pendulum).

The main catalyst for the development of chaos theory was the electronic computer. Much of the mathematics of chaos theory involves the repeated iteration of (simple) mathematical formulas, which would be impractical to do by hand. Computers made these repeated calculations practical, while figures and images made it possible to visualize these systems. In the 1960's Edward Lorenz an early pioneer of chaos theory who worked on weather prediction [lor63], simulated his weather model on a computer. He realized, that small changes in initial conditions produced large changes in the long-term outcoming weather patterns. This sensitive dependence on initial conditions came to be known as the "butterfly effect". Lorenz's discovery showed that even detailed atmospheric modeling cannot in general make long-term weather predictions. Weather is usually predictable about a week ahead only! This surprising finding of Lorenz is an example for the relevance of studies of classical chaotic systems in understanding daily life problems. Probably this fact is the main reason why classical nonlinear dynamics

enjoy high popularity among the general public. Talking to non-physicists interested in my work, many of them had heard about the butterfly effect or have seen a double pendulum, but simply nobody has heard something about "Quantum Chaos", the field where the presented work is residing. Nevertheless even if you have no idea what it is it is "flavored" with "quantum" and "chaos", so simply (or only) the word attracts interest.

In his scholarpedia article Martin Gutzwiller [gut07] illustrates Quantum Chaos as: *'Building a bridge between Quantum Mechanics (QM) and Classical Mechanics (CM)'*, which provides a transition from QM to CM, as well as from CM to QM and whose existence puts limits on CM and on QM. On this bridge one studies the quantum mechanics of classically chaotic systems. Because Chaos in a classical sense does not exist in QM the more descriptive term 'quantum chaology' was proposed by Michael Berry [ber87], but it was not generally accepted. Quantum Chaos simply sounds better. As standard introduction and a detailed review on Quantum Chaos I refer to the monographs "Quantum Signatures of Chaos" by Fritz Haake [haa01] and "Quantum Chaos - An Introduction" by Hans-Jürgen Stöckmann [stoe99]. Talking to physicists who have already heard something about Quantum Chaos, they always connect this field with theoretical physics. Doing experiments in this field using so called microwave billiards is at least for most of these physicists completely unknown and a somehow strange field of research.

On Quantum Chaos only two classes of experimental results had been available till the 1990's. From nuclear physics the spectra of compound nuclei [por65] which are closely connected with the development of random matrix theory [wig55, meh63] and from atomic physics the experiments with highly excited hydrogen and alkali atoms in strong magnetic fields [hol86, mai86]. Then different experiments using classical waves have been performed, starting with so called microwave billiards [stoe90]. These are analogue experiments with microwave resonators to study the properties of quantum billiards. Other classical wave experiments have been performed with water surface waves on water vessels [blue92] or with vibrating blocks [ell95, lob03, gor06, lob08]. In all experiments classical waves are used to study questions which are often relevant for matter waves. That is why some authors prefer the term "wave chaos" [seb90, so95, tan07] to describe this experimental field of Quantum Chaos research. The basic concepts of these experiments are recapitulated in chapter 2. For an introduction in Quantum Chaos including billiard experiments with classical waves especially microwaves I refer to the book [stoe99]. A short overview also can be found in the scholarpedia article: on "Microwave billiards and Quantum Chaos" [stoe10].

Having adumbrated the field of research for the presented work I want to focus on the main topic: Sensitivity of quantum dynamics to perturbations. This important objective in the field of Quantum Chaos has been studied experimentally in this work. Measured by the overlap between time-evolved perturbed and unperturbed Hamiltonians with same initial state, as suggested by Peres [per84], stability of quantum time evolution has been studied from various viewpoints and under different names in the past. In the following equation

$$F(t) = |\langle\psi_2(t)|\psi_1(t)\rangle|^2 = |\langle\psi_0|e^{iH_2t/\hbar}e^{-iH_1t/\hbar}|\psi_0\rangle|^2 = |\langle\psi_{12}(t)|\psi_0\rangle|^2 = M(t) \qquad (1.1)$$

the main quantity of interest for this thesis is written explicitly. The equation can be described by two possible interpretations either the "fidelity" $F(t)$ or the "Loschmidt echo" (LE) $M(t)$.

The fidelity conciders the overlap of the quantum state $|\psi_1(t)\rangle = e^{-iH_1t/\hbar}|\psi_0\rangle$ obtained from an initial state $|\psi_0\rangle$ in the course of its evolution time t under a Hamiltonian H, with the state $|\psi_2(t)\rangle = e^{iH_2t/\hbar}|\psi_0\rangle$ that results from the same initial state by evolving the latter for the same time, but under a perturbed Hamiltonian H_2 different from H_1. The LE compares the overlap of the initial state $|\psi_0\rangle$ and the state $|\psi_{12}(t)\rangle$ obtained by first propagating $|\psi_0\rangle$ till t under the Hamiltonian H_1, and then backwards for the same time under H_2. The considered overlap equals unity at $t = 0$ and typically decays further in time.

In the field of quantum information fidelity plays an important role for quantifying the susceptibility of quantum dynamics to environmental or other external perturbations [nie00]. Quantum information theory enables one to do things not possible by classical means, e.g., perform quantum computation. The main obstacle in producing quantum devices that manipulate individual quanta are errors in the evolution, either due to unwanted coupling with the environment or due to internal imperfections. Therefore, the goal is to build a device that is resistant to such perturbations. For this one ought to understand the behaviour of fidelity in different situations to know how to maximize it for the time duration of the calculation. The fidelity for this case needs to be of the order $F \approx 0.9999$ [nak06]. Using error correction maybe 0.999 might be sufficient.

In semiclassical quantum and wave mechanics the terminus LE is often used [usa98] especially for Hamiltonians associated with complex, in particular classically chaotic dynamics. The terminology refers to the notion of echoes from momenta reversal in a Hamiltonian system considered by Loschmidt [los76] in the 19th century. The sensitivity to perturbations as measured by the LE allows for the comparison between quantum and classical situation. For classical systems LE gives the same exponential sensitivity to perturbations of the evolution as to perturbations of initial conditions, whereas for quantum system the LE can behave in a very different way, displaying a rich variety of regimes. Depending on the nature and strength of the perturbation for fully chaotic systems there are three prominent LE/fidelity decay regime, the perturbative Gaussian, the Fermi-golden-rule(FGR) and the Lyapunov regime [jac01, jal01, cer02, cuc02]. In all this references so called "global" perturbations have been considered, that means that there is a total rearrangement of spectrum and eigenfunctions already for moderate perturbation strength, or in a semiclassical picture, that the Hamiltonian perturbation affects every trajectory of the system, and therefore all trajectories are responsible for the decay of the LE.

Experiments with microwave cavities or elastic bodies seem to provide good options to study the decay of fidelity [sch05a], but a difficulty arises. Fidelity implies an integration over the entire space. In two-dimensional microwave billiards the antenna always represents a perturbation, and thus moving the antenna defeats the purpose of a fidelity measurement, as the wave-function taken at any point is that of a slightly different

system. In contrast to wave function measurements, in fidelity experiments we are precisely interested in such differences, and thus wave functions measured with moveable antennas [ste92, ste95, kuh07] or a moveable perturbation bodies [sri91, bog06, lau07] are not appropriate. In elastic experiments on solid blocks [lob03, gor06, lob08] or 3D microwave billiards the wave function inside the volume seems to be inaccessible anyway [doer98, alt97]. This lead to the development of the concept of scattering fidelity [sch05a] which tests the sensitivity of S-matrix elements to perturbations and equals the ordinary fidelity for fully chaotic systems and weak coupling. This is also of intrinsic interest, since the scattering matrix may be considered as the basic building block at least in the case of quantum theory [str00, leh55].

In former studies the scattering fidelity has been investigated in chaotic microwave billiards by considering a perturbation of the billiard interior. It can be shown that in such a case the random character of wave functions causes the scattering fidelity to represent the usual fidelity, provided that appropriate averaging is taken [sch05a, hoeh08]. Scars and parabolic manifolds will obviously change that correspondence, but their effect can be avoided in experiments [sch05a]. Specifically, two different types of interior perturbations were experimentally studied. In the first set of experiments a billiard wall was shifted, realizing the so-called global perturbation [sch05a, sch05b], meaning that there is a total rearrangement of both spectrum and eigenfunctions already for moderate perturbation strengths. A good agreement with predictions from random matrix theory (RMT), expecting Gaussian or exponential decay depending on perturbation strength, was found. A theoretical and experimental investigation of fidelity decay for a type of "local" perturbations in the perturbative regime, where the eigenstates are not significantly modified by the perturbation, has been done in [hoeh08]. On the experimental side a small scatterer was shifted inside the microwave billiard in a two-dimensional array of point-like scatterers. Using the random plane wave conjecture, an algebraic decay $1/t$ was expected theoretically and confirmed experimentally.

In the present thesis the scattering fidelity decay is studied in a chaotic microwave billiard for two other types of local perturbations. In the first part of this thesis fidelity decay is studied in classically chaotic microwave billiards for a local, piston-like boundary perturbation. Experimentally a predicted non-monotonic cross-over from the Fermi Golden Rule to the escape-rate regime of the LE decay with increasing local boundary perturbation [gou08] is verified. In particular, a pronounced oscillation of the decay rate as a function of the piston position is observed, which quantitatively agree with corresponding theoretical results based on a refined semiclassical approach for local boundary perturbations. The presented results have been published in [koeb11]. In the second part the fidelity decay in a microwave billiard is considered, where the coupling to an attached antenna is varied. The resulting quantity, coupling fidelity, is experimentally studied for three different terminators of the antenna: a hard wall reflection, an open wall reflection, and a $50\,\Omega$ load, corresponding to a totally open channel. Quantitative agreement is found with the theory obtained from a modified VWZ [ver85] approach. The main results presented in this part and a more detailed model description in terms of an effective Hamiltonian with a complex coupling constant developed by D.Savin have been published in [koeb10].

2 Fundamental concepts

2.1 Billiard systems

Classical billiards constitute an important class of dynamical systems. In classical billiard systems, a point particle is confined to a region in configuration space and collides with the boundary of the region such that the angle of incidence equals the angle of reflection. The systems dynamic depends on the shape of the billiard-boundary and can be completely described by the entirety of its periodic orbits. Depending on the billiard-shape one can distinguish different types of dynamics – so called *regular* dynamic, e.g. the distance between two phase space trajectories with similar initial conditions grows at most linear; and *chaotic* dynamic, where the distance between two phase space trajectories with similar initial conditions grows exponentiallly. The dynamics of most billiards is neither completely (i.e. for all initial conditions) regular nor completely chaotic, but is mixed.

For a quantum-mechanical treatment of billiard systems one can no longer use the classical characterisation of regular and chaotic behaviour in terms of trajectories, because of the Heisenberg uncertainty principle. A quantum billiard is described by the stationary Schrödinger equation of a free particle with Dirichlet boundary conditions.

Billiard systems demonstrate fundamental physical phenomena that can be observed in laboratory settings.

2.2 Microwave experiments

Microwave experiments with flat cavities are meanwhile a well-known paradigm in the field of Quantum Chaos [stoe99].

About 20 years ago in our group Stöckmann and Stein started microwave studies on irregular shaped metallic resonators (Fig. 2.1) with top and bottom plate parallel to each other [stoe90]. One can describe this systems by a two-dimensional electromagnetic wave equation (Helmholtz equation) with Dirichlet boundary conditions. As long as a maximum frequency $\nu_{\max} = c/(2h)$, where h is the height of the resonator and c denotes the speed of light is not surpassed a one-to-one correspondence to QM is given. The correspondence of the Helmholtz equation to the Schrödinger equation with same boundary conditions allows to study prediction for quantum billiards by means of flat

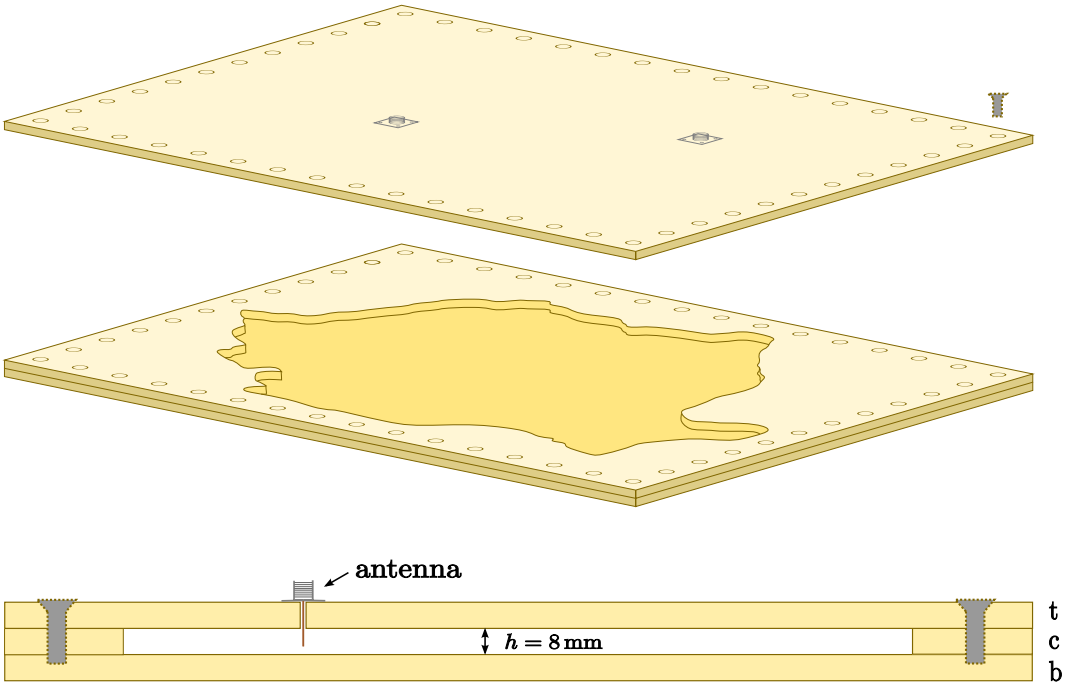

Figure 2.1: Sketch of a microwave resonator in exploded view (upper figure) and sectional drawing (lower figure). The resonator consist of a top (t), contour (c) and a bottom (b) plate made of brass. The shape of the microwave billiard is given by the contour plate, which in general is not a single plate. Antennas, which are introduced into the cavity through small holes, are used to fed in microwaves into the resonator. The height of the resonators, which have been used for all presented experimental works, is $h = 8\,\mathrm{mm}$.

microwave resonators, which are named microwave billiards. Fortunately, the correspondence named above is not restricted to closed systems, it includes the scattering situation as well. So it is possible to verify predictions from quantum-mechanical scattering theory by means of open microwave resonators with a number of attached open channels, either antennas or wave guides. All experimental studies presented in this work are based on this correspondence.

2.3 Scattering formalism

In nuclear physics much insight is gained by performing nuclear reaction experiments using particle accelerators. The principle of these experiments can be described as a three-step process. In a first step an accelerated particle is moving towards the reaction target. Ideally all quantum numbers (spin, parity, momentum, etc.) are known. This set of numbers labels the incident channel. In a second step the particle hits the target, that means, it interacts locally with some potential which might cause some of the quantum numbers to change. In the third and final step a particle leaves the interaction region to

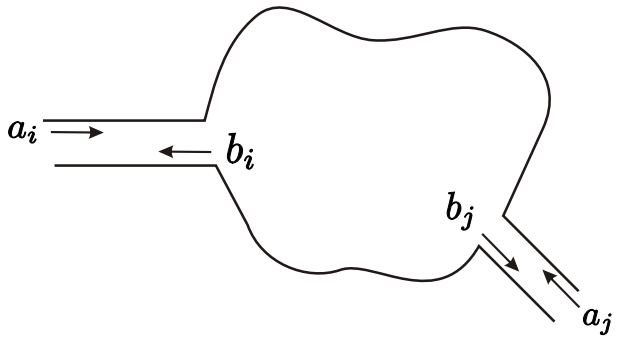

Figure 2.2: Sketch of scattering system to demonstrate the notation of incoming and outgoing waves

be registered by some detector system that determines the new set of quantum numbers which now labels the final channel. This whole process defines a scattering problem where the fundamental challenge is to determine the transition probability from a given initial channel to a given final channel.

In our experiments microwaves are fed into the resonator using antennas, which are introduced into the cavity through a small hole. The reflection and transmission properties between different antennas are described by the scattering matrix S It is defined by

$$b = Sa\,, \tag{2.1}$$

where $a = (a_1, a_2, \cdots)$ is the vector of amplitudes of the waves entering through the different channels and $b = (b_1, b_2, \cdots)$ is the amplitude vector of the outgoing waves. The diagonal elements S_{ii} of S correspond to the reflection amplitude at antenna i, whereas the non diagonal elements S_{ij} are related to the transmission amplitude between antenna i and j (Fig. 2.2). Microwave experiments allow measuring of the complete scattering matrix including the phases in frequency space using a vector network analyser (VNA).

The following expression which gives a connection between the Hamiltonian H of the system and the scattering matrix S was initially developed in nuclear physics [mah69, ver85, sok89]:

$$S(E) = 1 - 2iW^{\dagger}\frac{1}{E - H_{\text{eff}}}W, \tag{2.2}$$

where W discribes the coupling between the internal Hamiltonian H and the scattering channels. The coupling modifies H to become an effective Hamiltonian

$$H_{\text{eff}} = H - iWW^{\dagger} \tag{2.3}$$

in Eq. (2.2). It should be noted that the scattering matrix is in general a complex valued object and in nuclear physics only the cross section, that is its modulus square, is experimentally accessible. Eq. (2.2) provides the crucial connection between theory and measurement. It links the information of the scattering matrix obtained in experiments to the Hamiltonian which is of interest to theoretical considerations. For quantum systems exhibiting chaotic dynamics the Hamiltonian can be described using Random Matrix

Theory (RMT). The couplings W are given parameters of the problem and are often assumed to follow a Gaussian distribution. A possible energy dependence of W is often neglected. Using this universal description of a scattering process, Eq. (2.2) allows for predictions of statistical properties of the scattering matrix. This approach in Eq. (2.2) has been successfully applied to study various aspects of open systems, including wave billiards [stoe99, fyo97, dit00, fyo05].

2.4 Scattering fidelity

Fidelity, as it is usually defined (Eq. (1.1)), also applies to scattering systems. A wave packet can be evolved with two slightly different scattering Hamiltonians. This would be the standard fidelity of a scattering system. In contrast, "scattering fidelity" stands for a quantity which can be obtained from simple scattering data, though under certain conditions it agrees with the standard fidelity.

We now proceed with the introduction of the concept of scattering fidelity. In microwave experiments we can measure scattering matrix elements for unperturbed ($S_{ab}(\nu)$) and perturbed ($S'_{ab}(\nu)$) systems independently in frequency space. By taking the Fourier transform

$$\hat{S}_{ab}(t) = \int d\nu \, e^{2\pi\imath\nu t} S_{ab}(\nu) \tag{2.4}$$

of any scattering matrix element we obtain $\hat{S}$, the scattering matrix in the time domain. This leads to the definition of the scattering fidelity amplitude [sch05a]:

$$f_{ab}(t) = \frac{\langle \hat{S}_{ab}(t)\hat{S}'^{*}_{ab}(t)\rangle}{\sqrt{\langle \hat{S}_{ab}(t)\hat{S}^{*}_{ab}(t)\rangle \langle \hat{S}'_{ab}(t)\hat{S}'^{*}_{ab}(t)\rangle}} \,. \tag{2.5}$$

This definition ensures that $f_{ab}(0) = 1$. Furthermore, an overall decay of the correlation functions due to absorption or other open channels drops out, provided the decay is the same for the parametric cross-correlation functions in the nominator and the autocorrelation functions in the denominator. The scattering fidelity itself is

$$F(t) = |f_{ab}(t)|^2 \,. \tag{2.6}$$

For chaotic systems and weak coupling of the measuring antenna the scattering fidelity approaches the ordinary fidelity (Eq. (1.1)) [sch05a].

3 Fidelity decay for local boundary perturbation

3.1 Introduction

In Ref. [gou07] Goussev and Richter extend the original semiclassical approach to the Loschmidt echo (LE) [jal01, cuc02] to *strong local* perturbations in coordinate space. Analytically they found a new LE decay for chaotic billiards with a local boundary deformation where the LE decays exponentially in time, with a rate which equals to the classical "escape rate" from a related open billiard. This open billiard is obtained from the original one by removing the perturbation-affected region of its boundary. Goussev and Richters' numerical study was performed for a desymmetrized diamond (DD) billiard and showed a good agreement with an analytical decay law $\exp(-2\gamma t)$, where γ is the classical "escape rate" from the related open billiard. A generalization of this approach to weak perturbations was published in [gou08] and predicted a non-monotonic cross-over from the Fermi-golden-rule regime to the escape-rate regime with increasing perturbation strength. For a special type of billiard's boundary deformation, where the area of deformation is increased by an imaginary "piston" pulled out of the billiard, the LE decay rate is expected to show oscillations as a function of the piston position (perturbation strength). Numerically the predicted crossover has been verified for maps [are09]. In quantum wave packet simulations for billiards only precursors of this behaviour could be found [gou08]. An experimental verification of the predicted oscillations using microwave billiards will be presented in this chapter. The main results have been already published in [koeb11].

3.2 Theory

Here I want to give a short outline of the main theoretical results needed for the interpretation of the experiments. A detailed derivation can be found in the following articles [gou07, gou08, koeb11]. In the semiclassical regime one can write for the LE approximately

$$M(t) \approx e^{-\kappa\gamma t} \tag{3.1}$$

neglecting the contribution of a diagonal part to the LE [gou08]. In the effective decay rate $\kappa\gamma$ the dimensionless κ can be expressed as

$$\kappa = 2\left(1 - \mathrm{Re}\langle e^{2\pi i u/\lambda}\rangle\right) . \tag{3.2}$$

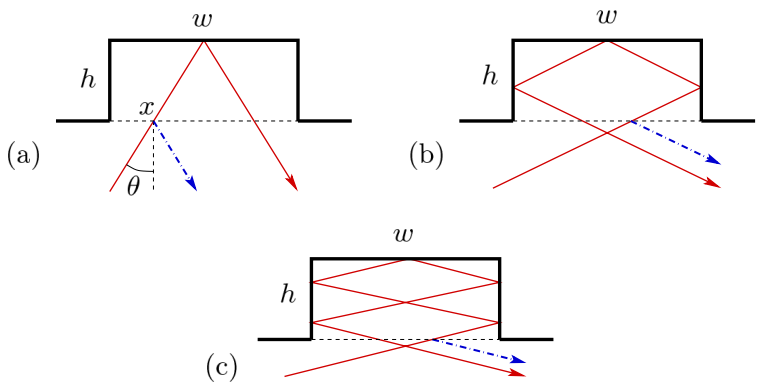

Figure 3.1: Piston-like boundary deformation with examples of correlated trajectory pairs, unperturbed (blue) and perturbed (red), belonging to sets Ω_1 (a), Ω_3 (b) and Ω_5 (c). Origin: [koeb11]

In this expression for κ we call u the deformation function. This deformation is given by the difference in the length between the perturbed trajectory and the unperturbed one. While the perturbation is introduced by the local deformation of the chaotic billiards boundary. Dividing out the de Broglie wavelength λ the deformation is rescaled to units of the de Broglie wavelength. Now we look at a special type of boundary deformation, where the area of deformation has the shape of a rectangle which can be varied at one side by a "piston" (Fig. 3.1). This corresponds exactly to the experimental realisation of the perturbation (see Sec. 3.3.1). For a piston width w and displacement h of the piston, the expression (3.2) can be calculated in the limit $h \ll w$ (see [gou08]) up to the following expression

$$\kappa = \pi \mathbf{H}_1(4\pi h/\lambda), \tag{3.3}$$

where $\mathbf{H}_1$ is the Struve H-function of first order. For arbitrary w and h this can be generalized to

$$\kappa = 2 - \frac{2}{w} \sum_{k=0}^{\infty} \int_{\Omega_{2k+1}} \mathrm{d}x \, \mathrm{d}\theta \cos\theta \cos\left[\frac{4\pi}{\lambda}\left(h\cos\theta + kw\sin\theta\right)\right] \tag{3.4}$$

with the integration domains Ω_{2k+1} over incident positions x and momentum directions θ (see Fig. 3.2). Detailed calculation can be found in the appendix of [koeb11]. This expression can be evaluated numerically. Furthermore, the expression for the LE in Eq. (3.1) depends on the classical escape rate γ which belongs to the corresponding open billiard if the local piston deformation is completely removed from the boundary region. The escape rate is given by

$$\gamma = \frac{p_0}{m l_d}, \tag{3.5}$$

where p_0 denotes the momentum and m denotes the mass of a classical particle, while l_d stands for the average dwell length. The later one is determined by the length of paths in the related open chaotic billiard obtained from the original (closed) one by removing the boundary region. For billiards, where the deformation widths ("openings") w are

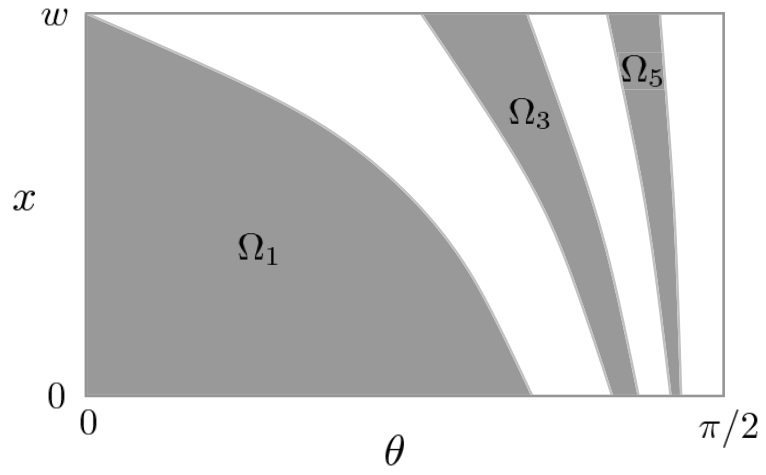

Figure 3.2: Schematic representation of the regions Ω_1, Ω_3, and Ω_5, see text. Further regions, Ω_{2k+1} with $k \geq 3$, contributing to the sum on the right hand side of Eq. (3.4) are not shown in the figure; they cluster as narrow stripes "to the right" of Ω_5 and approach $\theta = \pi/2$ in the limit $k \to \infty$. Origin: [koeb11]

much smaller than the perimeter of the closed billiard one can approximate the average dwell length $l_d \approx \pi A/w$ where A is the area of the corresponding closed billiard. For comparison with our experimental data from microwave billiards, p_0/m is set to the speed of light c and therefor the corresponding escape rate can be determined as

$$\gamma \approx c\frac{w}{\pi A}. \tag{3.6}$$

The perturbation strength, as the main parameter-dependences of the Loschmidt echo, is in semiclassical theory measured by the action change which results from the perturbation. So in our chaotic billiard systems with piston-like boundary deformation the displacement h of the piston is the parameter which introduces the perturbation strength.

For the perturbation strength it proves convenient (see Ref. [gou08]) to define the dimensionless quantity

$$\chi = 2\pi\sqrt{\langle u^2\rangle}/\lambda, \tag{3.7}$$

depending on square-root of second moment of the deformation function u in units of the de Broglie wavelength λ. For a piston-type deformation the dimensionless perturbation strength reads

$$\chi = 2\pi\sqrt{(8/3)}h/\lambda, \tag{3.8}$$

which is simply a rescaled displacement h in units of λ.

Depending on the perturbation strength χ based on the Eqs. (3.1, 3.2) one can identify different decay regimes of the LE. For a weak local perturbations, $\chi \leq 1$, the LE decays like

$$M(t) \approx e^{-\chi^2\gamma t}, \quad (\chi \leq 1) \tag{3.9}$$

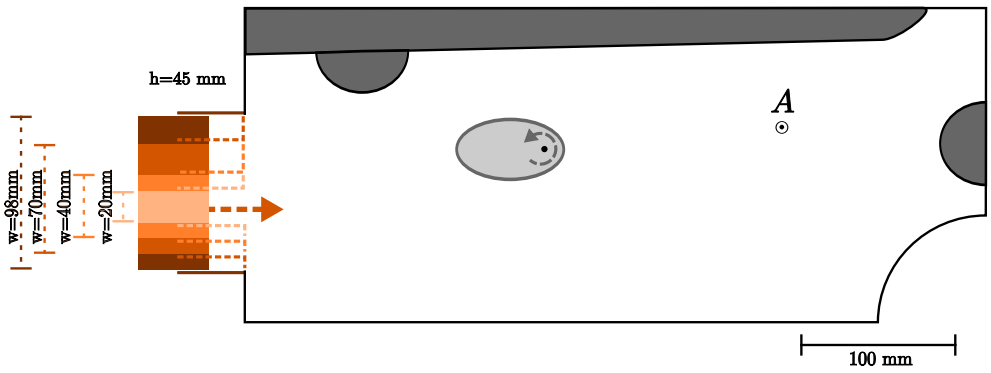

Figure 3.3: Sketch of the chaotic Sinai-shaped billiard (length of 472 mm, width of 200 mm and a quarter-circle of radius of 70 mm) with a variable piston-like local boundary deformation. The piston position can be changed from a displacement $h = 45\,\text{mm}$ to $h = 0\,\text{mm}$ for four different piston widths $w = 20, 40, 70, 98\,\text{mm}$. At position a the measuring antenna is introduced. The additional elements were inserted to perform ensemble averages (rotatable ellipse) and to reduce the influence of bouncing balls.

so the rate of the exponential decay depends on the perturbation strength χ, in analogy to the Fermi Golden Rule regime found for global perturbations. On the other hand, in the limit of strong local perturbations, $\chi \gg 1$,

$$M(t) \approx e^{-2\gamma t}, \quad (\chi \gg 1) \tag{3.10}$$

the LE decay rate is independent of perturbation strength χ. The correspondence to the escape rate regime is presented in [gou07].

In the following section we will use Eq. (3.1), together with the expressions (3.3) and (3.4) for the decay rate κ, for a comparison with the experimentally determined scattering fidelity (Eq. (2.6)).

3.3 Experiment

3.3.1 Experimental setup

Our experiment has been done with a microwave resonators of height of 8 mm which can be treated as a two-dimensional billiard system for frequencies below 18 GHz. In Fig. 3.3 the geometry of the setup is illustrated. The basic shape is a quarter Sinai billiard, where additional elements have been inserted to reduce the influence of bouncing-ball resonances. This leads to a classical dynamics of the billiard which is chaotic. For introducing the boundary deformation the straight left boundary of the unperturbed billiard was modified. Different pistons of four widths w have been attached successively to the billiard which allow for a variation of the escape rate γ (Eq. (3.5)). Each piston

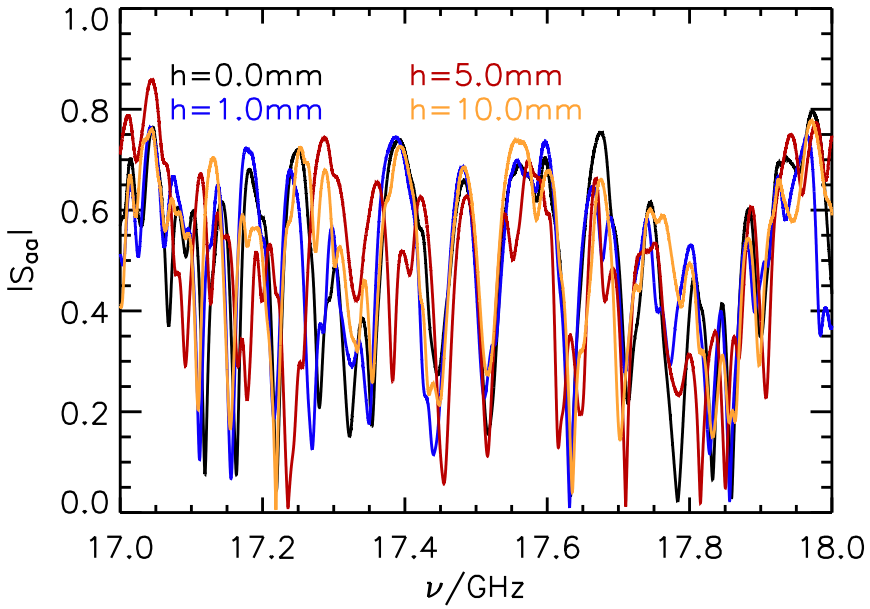

Figure 3.4: Reflection $|S_{aa}|$ for $w = 40\,\mathrm{mm}$ for different displacements h in a frequency range from 17 to 18 GHz.

position can be varied horizontal in steps of 0.5 mm via a step motor from a displacement $h = 45\,\mathrm{mm}$ to $h = 0\,\mathrm{mm}$, so the perturbation strength h respectively χ can be controlled changing the area of deformation. To perform ensemble averages a rotating ellipse (see Fig. 3.3) is inserted to the billiard. For measuring the reflection S-matrix element S_{aa} at position a an antenna is fixed and connected to an Agilent 8720ES vector network analyser (VNA). The measurement was done in a frequency range from 2 to 18 GHz with a resolution of 0.1 MHz for four piston widths and all displacements h realizing 18 different positions of a rotating ellipse. The unperturbed system is defined as the one with the straight wall, corresponding to $h = 0\,\mathrm{mm}$.

3.3.2 Results and Discussion

From the experimentally determined scattering matrix elements S_{aa} the scattering fidelity is calculated with $h = 0\,\mathrm{mm}$ (billiard with straight wall) as unperturbed system and $h \neq 0\,\mathrm{mm}$ (billiard with boundary deformation) as perturbed system, using Eq. (2.6). Necessary averaging $\langle \cdots \rangle$ for the correlation functions in Eq. (2.6) has been performed in all cases by an ensemble of 18 system realisations with different positions of the rotating ellipse. The presented experimental results of the scattering fidelity decay for the piston-like boundary perturbation will now be compared with the theoretical predictions (Eqs. (3.1)-(3.4)) for LE decay for this specific type of perturbation. The presentation of our results start with exemplary chosen spectra of our measured data. Fig. 3.4 shows the

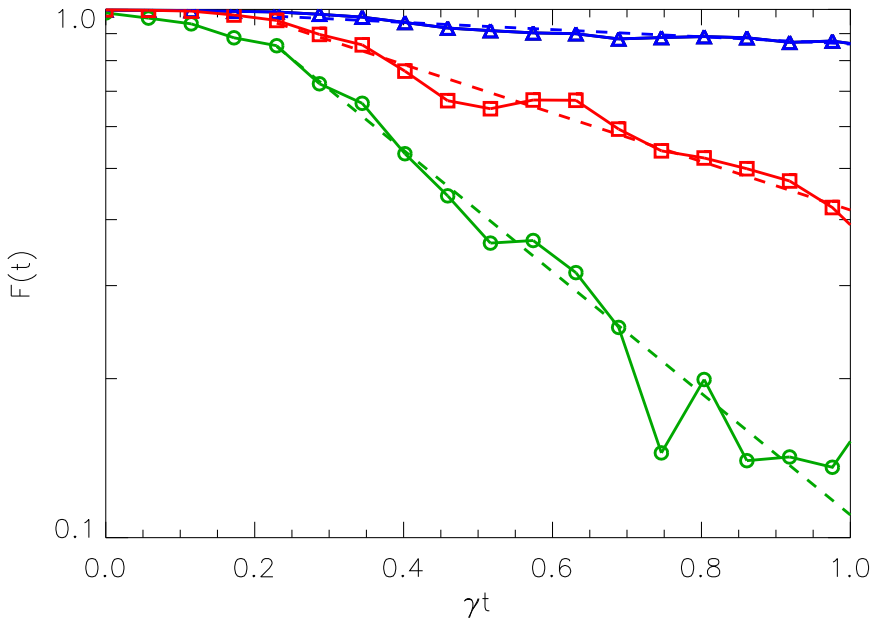

Figure 3.5: Measured scattering fidelity decay $F(t)$, Eq. (2.6), (solid lines with symbols) for three different piston displacements $h_1 = 1\,\text{mm}$ (triangles, blue), $h_2 = 5\,\text{mm}$ (circles, green), $h_3 = 10\,\text{mm}$ (squares, red), for a frequency range $17 - 18\,\text{GHz}$. The average frequency $\bar{\nu}$=17.5 GHz corresponds to a average de Broglie wavelength $\bar{\lambda} \approx 17\,\text{mm}$. The dashed lines show the corresponding semiclassical prediction, Eq. (3.1), for the LE decay, with κ chosen as free parameter: $\kappa_1 = 0.26$; $\kappa_2 = 2.78$; $\kappa_3 = 1.09$, respectively. The time is given in units of the dwell time $1/\gamma$, with γ determined from experimental parameters via Eq. (3.5) with $w = 40\,\text{mm}$.

absolute value of the reflection matrix element $|S_{aa}|$ as a function of frequency in a range from 17 to 18 GHz for a piston of width $w = 40\,\text{mm}$ in four different piston displacements h =0,1,5, and 10 mm. In the chosen frequency range we are in a regime of overlapping resonances. Thus we can not see shifts or broadening of single resonances. Comparing the results for the measurement of the billiard with the straight wall ($h = 0\,\text{mm}$) to the three spectra with boundary deformations ($h \neq 0\,\text{mm}$) we can state that over all the differences between the black line ($h = 0\,\text{mm}$) differs most from the red line ($h = 5\,\text{mm}$). But altogether the differences are rather small. So it is somehow surprising that we see such a clear difference in the scattering fidelity $F(t)$, Eq. (2.6), presented in Fig. 3.5, where the scattering fidelity $F(t)$ is plotted as symbols and solid lines exemplary for a piston of width $w = 40\,\text{mm}$ in three different piston displacements h =1,5, and 10 mm acting as perturbation to the system. As dashed lines the corresponding semiclassical prediction for the Loschmidt echo decay according to Eq. (3.1) are added. Parameter γ is always calculated via Eq. (3.6) using the corresponding geometrical parameter and constants, while κ is obtained by a fit to the experimental data. Beyond a certain time, which

passes until the perturbation is "seen" during the measuring process, a good agreement between the expected exponential law with LE decay exponent κ and the experimental fidelity decay is found. Increasing the displacements h, illustrated in Fig. 3.5 by the successive triangle (blue), circle (green) and squares (red) traces one can get a first idea of a non-monotonic behaviour of LE decay exponent κ with h, as the decay for the smaller perturbation (h =5 mm) is faster than the decay with larger perturbation (h =10 mm). Lets now take a closer look at the dependence of the Loschmidt decay exponent κ on the displacements h of the piston. In Figs. 3.6 (i)-(iv) for all four deformation widths w the decay rate κ is plotted as a function of deformations height h of the perturbed system. Coloured symbols in Fig. 3.6 (ii) at $h = 1,5$ and 10 mm mark data points $\kappa(h)$, obtained from fitting to the three cases of experimental fidelity decay which have been shown in Fig. 3.5. All asterisks show data points $\kappa(h)$ which have been obtained using the same procedure. In all four plots one can recognize an over all oscillating behaviour of the fidelity exponent which shows already a qualitatively good agreement with the predicted approximative theoretical result (Eq. (3.3)) depicted as dashed curve. But the data points do not exhibit that simple structure of monotonic decay of the maximum amplitude predicted by the approximate function (Eq. (3.3)). First of all there are obvious differences between all four widths which are not considered by the approximative theoretical result and will be discussed later together with the improved expression for κ (Eq. (3.4)) where the width w is no longer neglected. In particular for Fig. 3.6 (i) and (ii) the experimental results around $h \approx w$ (square shape of the piston-like deformation) and also $h \approx 2w$ in Fig. 3.6 (i) show a particularly pronounced amplitude which is not met by the dashed line at all. One can also see that for every width w there are some small but very specific deviations from the expected simple structure which are non generic. Having in mind that (Eq. (3.3)) is only valid for $h \ll w$, which is not reached even for the greatest width $w = 98$ mm the agreement between experiment and theory is already surprising. One can state that as expected from the approximation condition the deviations are smaller for larger w. But the second surprise is that this agreement was found far away from the semiclassical assumption, namely that the piston width w, should be much larger than the de Broglie wave length λ.

In all cases discussed up to now the average de Broglie wavelength had been $\bar{\lambda} \approx 17$ mm which corresponds to the average frequency $\bar{\nu}$=17.5 GHz of the chosen frequency range: $[17 - 18\,\text{GHz}]$. This is the smallest experimental realized de Broglie wave length and is not much smaller than w. Now we want to increase the average de Broglie wavelength looking for limits on the experimental side. Fig. 3.7 (i)-(iv) shows the decay rate κ as a function of the dimensionless rescaled perturbation strength χ (see Eq. (3.8)) for different de Broglie wave lengths λ in the three cases $w \geq 40$ mm. According to Eq. (3.3) the number of experimental accessible oscillations of $\kappa(h)$ up to $h_{max} = 45$ mm gets smaller for larger λ, this can be nicely seen in all plots of Fig. 3.7 (i)-(iv). Depending on the deformation width w there is a more ($w = 98$ mm) or less (w =20 and 40 mm) sharp value for λ where the over all amplitudes of $\kappa(\chi)$ do not any longer achieve the expected level. This region is achieved for w =20 and 40 mm for smaller de Broglie wave lengths ($\lambda \approx 20$ and 30 mm) and for $w = 98$ mm for larger de Broglie wave lengths ($\lambda \approx 60$ mm). The explanation for this behaviour is connected to the fact that the piston-like boundary

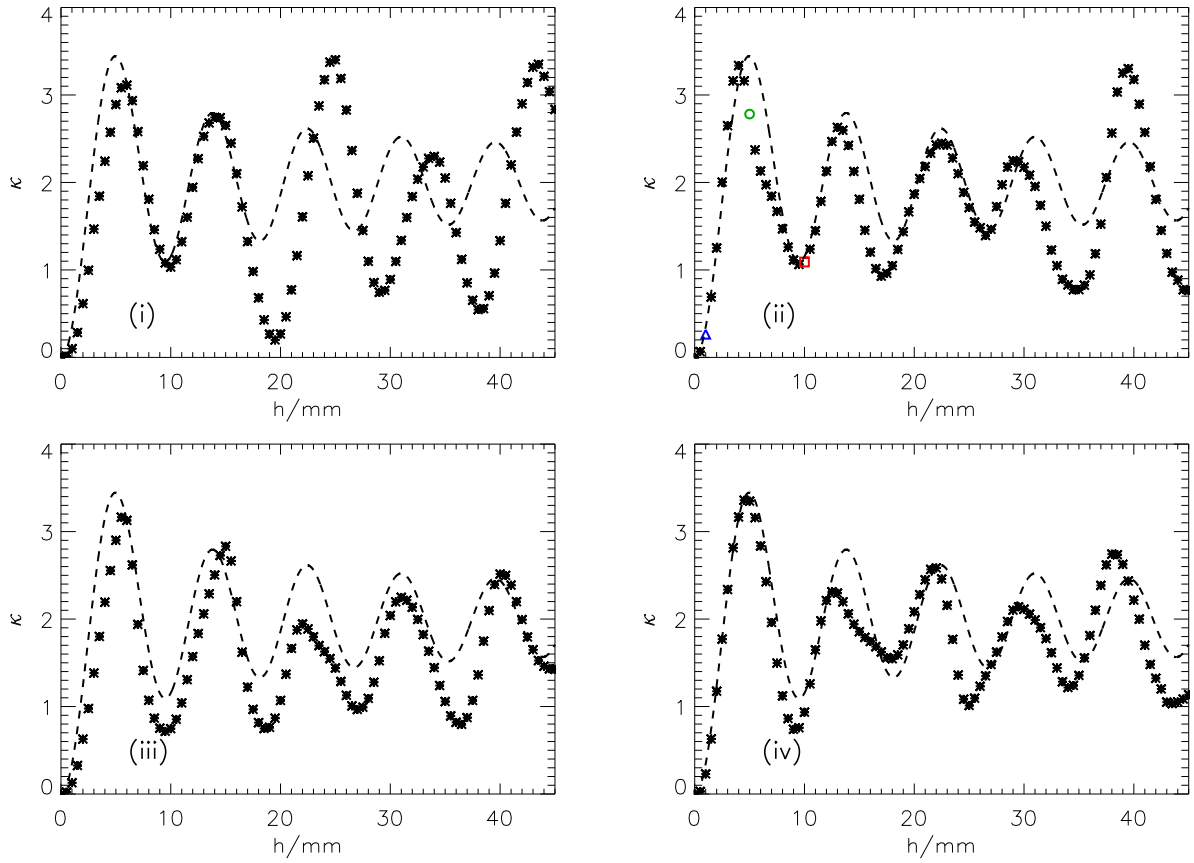

Figure 3.6: κ as a function of piston displacement h for pistons of width $w = 20\,\mathrm{mm}$ (i), $w = 40\,\mathrm{mm}$ (ii), $w = 70$ (iii) and $w = 98\,\mathrm{mm}$ (iv) for a average de Broglie wavelength $\bar{\lambda} \approx 17\,\mathrm{mm}$ [$17 - 18\,\mathrm{GHz}$]. The asterisks represent the data points obtained from fitting the decay exponent of the measured scattering fidelity. The three cases discussed in Fig. 3.5 are marked in (ii) by correspondingly colored symbols. The dashed curve shows the theoretical approximation (Eq. (3.3)) (valid for $h \ll w$).

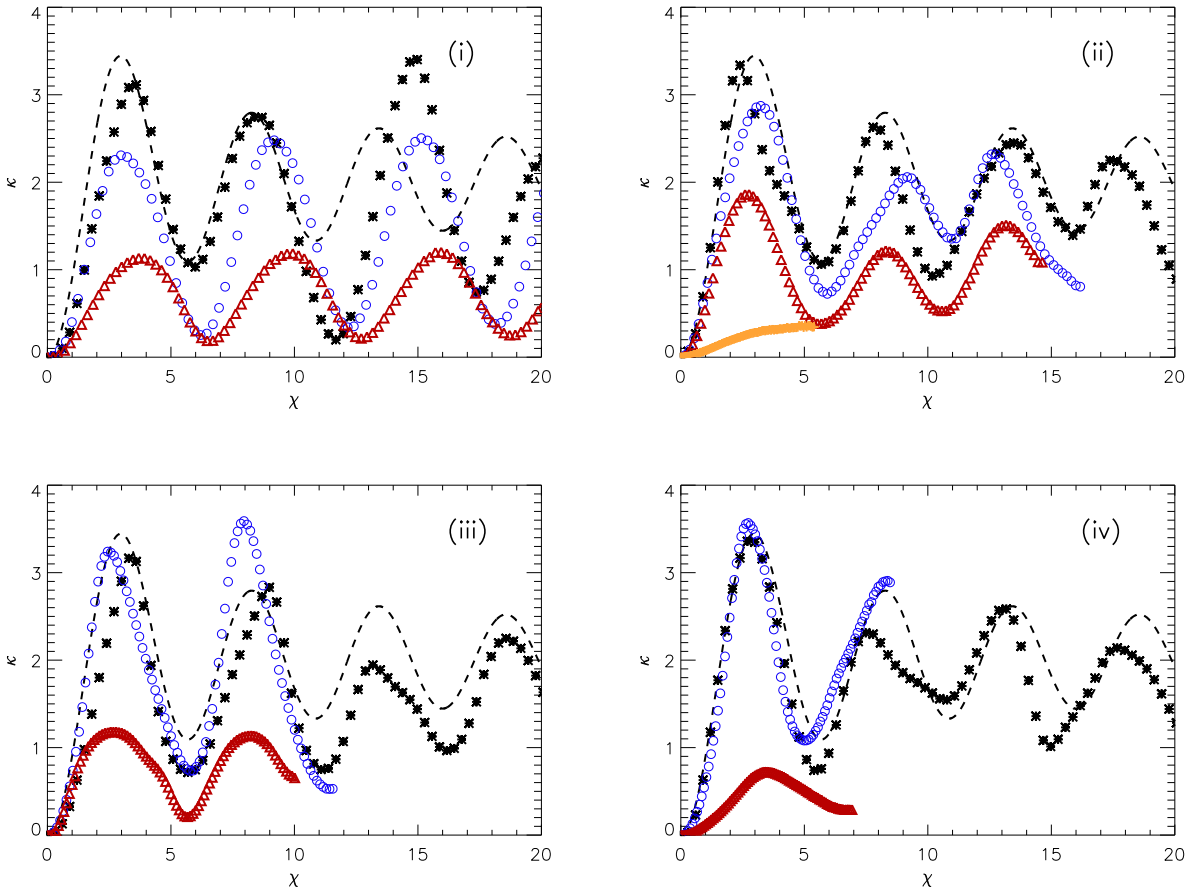

Figure 3.7: κ as a function of χ (Eq. (3.8)) for pistons of width $w = 20\,\mathrm{mm}$ (i), $w = 40\,\mathrm{mm}$ (ii), $w = 70$ (iii) and $w = 98\,\mathrm{mm}$ (iv). The asterisks (black) represent the data points for a average de Broglie wavelength $\bar{\lambda} \approx 17\,\mathrm{mm}$ $[17 - 18\,\mathrm{GHz}]$ (i)-(iv); the circles (blue) stand for $\bar{\lambda} \approx 21\,\mathrm{mm}$ $[14 - 15\,\mathrm{GHz}]$ (i); $\bar{\lambda} \approx 29\,\mathrm{mm}$ $[10 - 11\,\mathrm{GHz}]$ (ii); $\bar{\lambda} \approx 40\,\mathrm{mm}$ $[7 - 8\,\mathrm{GHz}]$ (iii); $\bar{\lambda} \approx 55\,\mathrm{mm}$ $[5 - 6\,\mathrm{GHz}]$ (iv) and the triangles (red) stand for $\bar{\lambda} \approx 22\,\mathrm{mm}$ $[13 - 14\,\mathrm{GHz}]$ (i); $\bar{\lambda} \approx 32\,\mathrm{mm}$ $[9 - 10\,\mathrm{GHz}]$ (ii); $\bar{\lambda} \approx 46\,\mathrm{mm}$ $[6 - 7\,\mathrm{GHz}]$ (iii); $\bar{\lambda} \approx 67\,\mathrm{mm}$ $[4 - 5\,\mathrm{GHz}]$ (iv). The crosses (orange) in (ii) stand for $\bar{\lambda} \approx 85\,\mathrm{mm}$ $[3 - 4\,\mathrm{GHz}]$. The dashed curve shows the theoretical prediction (Eq. (3.3)).

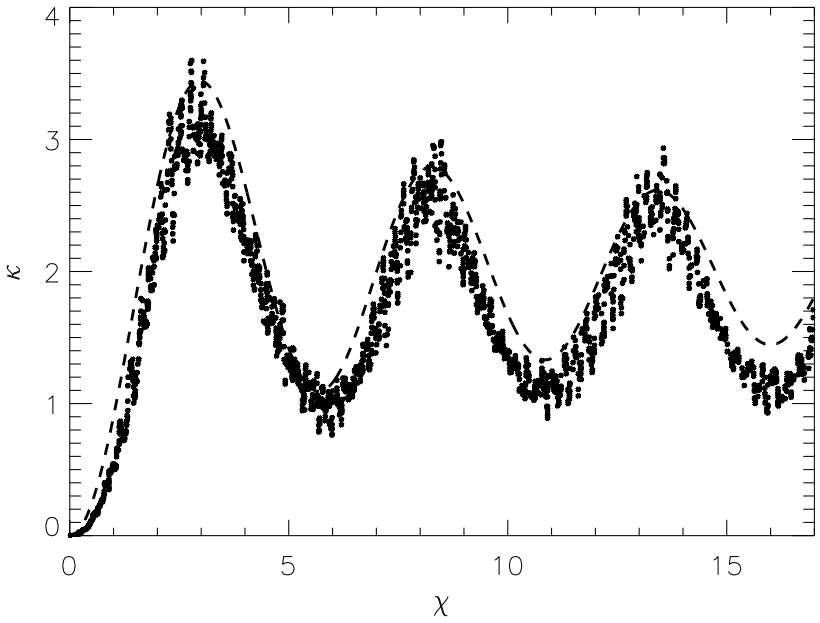

Figure 3.8: κ as a function of χ (see Eq. (3.8)). The fuzzy trace depicts the overlayed experimental data and the dashed curve the theoretical prediction (Eq. (3.3)).

deformation can only be seen from the waves starting inside the billiard if their wave length λ is smaller than twice the deformation width w. But also the amplitudes start breaking down the oscillations in the remaining data points remain until $\lambda \approx 2w$ as one can see in Fig. 3.7 (ii) (orange crosses). In the case $w = 20\,\mathrm{mm}$ (Fig. 3.7 (i)) one can see in all three experimental curves that the oscillation period does not agree with the theoretical expected result but as the theoretical approximation is only valid if the deformation height is small compared to the deformations width this deviation is not surprising.

In Fig. 3.8 we now superimpose all our experimental data points from $\kappa(\chi)$ curves which lie in the region where the average de Broglie wavelength $\bar{\lambda}$ is in the range $\bar{\lambda} < 2w$, $w \geq 40\,\mathrm{mm}$ and $h < w$. As a result we find a very convincing agreement with the approximative theoretical prediction (Eq. (3.3)) in the limit $h \ll w$.

Finally, we want to demonstrate that the agreement between the experimental and theoretical curves can be improved but we will also arrive at certain limits if the experimental conditions are pushed too far beyond the main limit of the semiclassical theory, $\lambda \ll w$. In Fig. 3.9 (i)-(iv) we plotted the same sets of experimental data as in Fig. 3.6 and added the second (exact) semiclassical results for κ) resulting from the numerical evaluation of the expression (3.4) as solid (red) line in addition to the already plotted in Fig. 3.6 dashed approximative result (Eq. (3.3)). Comparing only the theoretical results one see that for the approximative results the maximum amplitudes of κ decay monotonic with h while the full semiclassical results show an increase of the amplitudes of κ around $w = h$

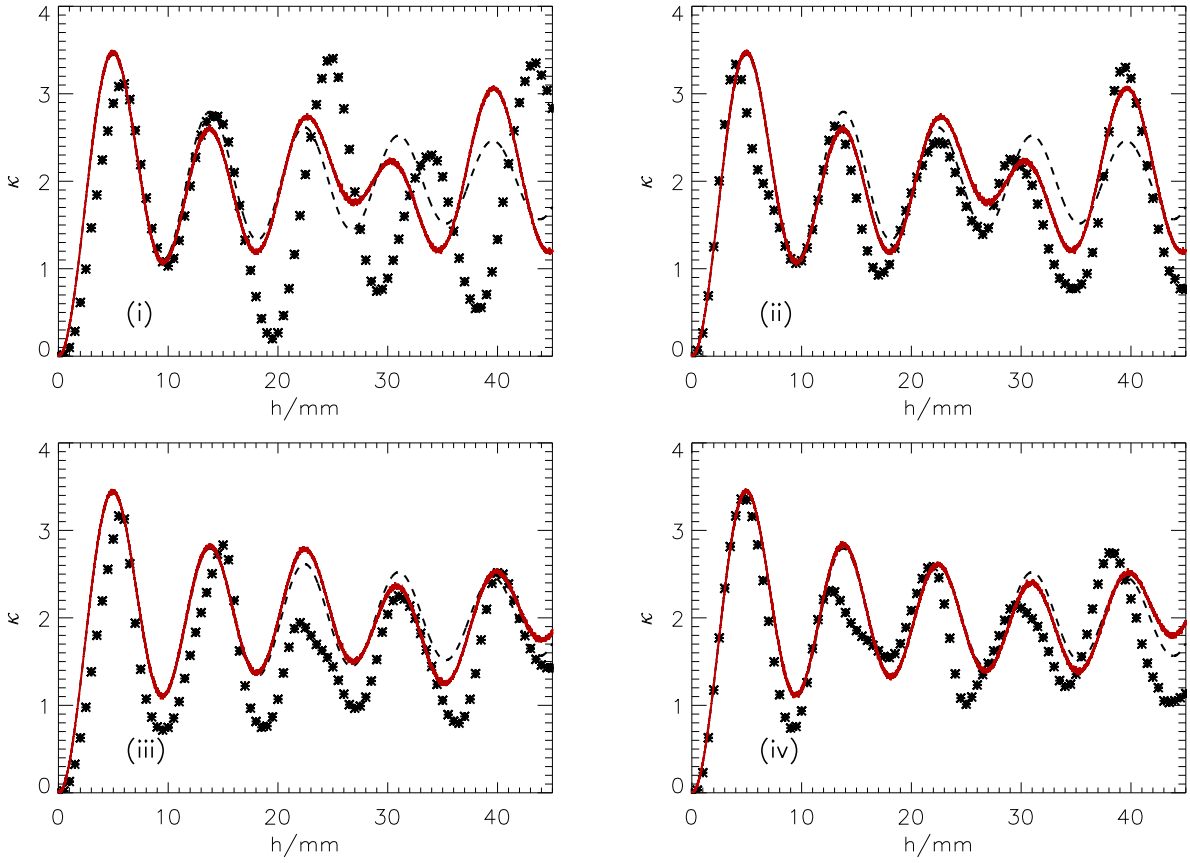

Figure 3.9: κ as a function of piston displacement h for a pistons of width $w = 20\,\mathrm{mm}$ (i), $w = 40\,\mathrm{mm}$ (ii), $w = 70$ (iii) and $w = 98\,\mathrm{mm}$ (iv) for a average de Broglie wavelength $\bar{\lambda} \approx 17\,\mathrm{mm}$ $[17 - 18\,\mathrm{GHz}]$. The asterisks represent the data points obtained from fitting the decay exponent of the measured scattering fidelity. The three cases discussed in Fig. 3.5 are marked in (b) by correspondingly colored symbols. The dashed curve shows the theoretical approximation (Eq. (3.3)) (valid for $h \ll w$), and the solid (red) curve is a result of the numerical evaluation of the full semiclassical expression (3.4).

which nicely can be seen in Fig. 3.9 (i) and (ii). One can state that the full theoretical expression describes the experimental situation more convincingly in all cases, while the difference between the full and the approximative theoretical result is pronounced in the case of a piston width $w = 20\,\mathrm{mm}$ and gets smaller with increasing piston width. In particular, for $h \approx w = 40\,\mathrm{mm}$ (square shape of the piston-like deformation) the experimental results show a particularly pronounced amplitude which is met by the solid line. But even if there is some improvement especially for the cases $w = 20\,\mathrm{mm}$ and $w = 40\,\mathrm{mm}$ concerning the regime around $h \approx w$ in Fig. 3.9 (i),(ii) (square shape of the piston-like deformation) and $h \approx 2w$ in Fig. 3.9 (i), the agreement is not really satisfying. For piston width $w = 20\,\mathrm{mm}$ which is of the order of $\bar{\lambda}$ the experimental data points (asterisks) even oscillate with a period that differs from the theoretical one. However, the fact that the experimental parameters are beyond the regime of validity of the semiclassical theory does not allow for a further reasonable comparison between experiment and theory.

4 Fidelity studies by varying the coupling

4.1 Introduction

The question how a physical system is perturbed during a measuring process seems to be one of the crucial things, that every experimentalist has to care about. In every laboratory efforts are made to perform experiments where the measurements perturb the original system property only as slightly as possible. Thinking about fidelity in the context of realizing quantum computers as a quantity which describes the stability of quantum time evolution, it seems quite natural to study fidelity under a type of perturbation which mimics the measuring process. When one opens a system it couples to the continuum with the consequence that the discrete energy levels transform into unstable resonance states. Varying the coupling strength to the scattering channels one can see rich dynamics [sok92], which have also been studied with microwave billiards [per00]. In this chapter I want to present our studies on the so called coupling fidelity focussing on the experimental part of the work. The main results including more detailed theoretical considerations have been published in [koeb10].

4.2 Theory

A short outline of the main theoretical results which can be found in more detailed derivation in [koeb10] will be given in this section.

4.2.1 The generalized VWZ approach to fidelity

The effective non-Hermitian Hamiltonian can be written as

$$H_{\text{eff}} = H - i\sum_{k=1}^{M} \lambda_k V_k V_k^{\dagger}\,, \qquad k \in \{1, \cdots, N\}\,; \tag{4.1}$$

with H the internal Hamiltonian of the closed system and V_k the coupling vectors (M scattering channels connected to N levels of the closed cavity) containing the information on the coupling of the levels to the continuum. We assume the V_k to be normalized to one, so λ_k is the coupling constant of channel k. The phenomenological coupling constant λ_k which enters the final expression Eq. (4.7) via the transmission coefficients

$$T_k = \frac{4\lambda_k}{(1+\lambda_k)^2} \in [0,1] \tag{4.2}$$

are usually taken as real numbers as their imaginary part can be absorbed in the Hamiltonian. For a suitable description of the experiments (see Sec. 4.3.1 and Sec. 4.3.2), which have been performed for varying the coupling to the system, in general one has to use complex numbers for the coupling constant of the varied (perturbing) channel. So all coupling constants λ_k will be treated as complex numbers ($\mathrm{Re}(\lambda_k) \geq 0$, due to the causality condition of the S-matrix). Rewriting Eq. (2.2) for the S-matrix at the scattering energy E in terms of H_{eff} with complex coupling constants $\lambda_{a,b}$ we get the following expression:

$$S_{ab}(E) = \delta_{ab} - 2i\sqrt{\mathrm{Re}(\lambda_a)\mathrm{Re}(\lambda_b)}\, V_a^\dagger \frac{1}{E - H_{\mathrm{eff}}} V_b \,. \tag{4.3}$$

The reflection amplitude S_{ll} in an arbitrary channel can be written as [fyo05]

$$S_{ll}(E) = \frac{1 - i\lambda_l^* V_l^\dagger \frac{1}{E - H_{\mathrm{eff}}^l} V_l}{1 + i\lambda_l V_l^\dagger \frac{1}{E - H_{\mathrm{eff}}^l} V_l} \,. \tag{4.4}$$

which is more suitable for our situation. It is obtained from Eq. (4.3) by single out the contribution to H_{eff} due to channel l writing $H_{\mathrm{eff}} = H_{\mathrm{eff}}^l - i\lambda_l V_l V_l^\dagger$ with $H_{\mathrm{eff}}^l = H - i\sum_{k\neq l} \lambda_k V_k V_k^\dagger$ (For details see in [koeb10]). It is convenient to use representation (Eq. (4.4)) to perform statistical averaging. With $E = 0$ this calculation leads to the following expression for the average S-matrix [ver85, sok89]:

$$\langle S_{ll} \rangle = \frac{1 - \lambda_l^*}{1 + \lambda_l} \tag{4.5}$$

and the transmission coefficient,

$$T_l \equiv 1 - |\langle S_{ll} \rangle|^2 = \frac{4\,\mathrm{Re}(\lambda_l)}{|1 + \lambda_l|^2} \,, \quad l = 1, \ldots, M \tag{4.6}$$

which agrees with the result of Ref. [ver85]. For the case of a real coupling constant Eq. (4.2) gives a transmission coefficient while for pure imaginary coupling constant which corresponds to perfect reflection at a closed channel the transmission coefficient equals zero.

4.2.2 Coupling Fidelity

We will now introduce a special type of scattering fidelity (see Eq. (2.5)), where the perturbation to the system is achieved by changing the complex coupling strength of one (perturbing) channel. This one is different from the channels a, b, which where used to measure the S Matrix elements for calculating the scattering fidelity. For this scattering fidelity which will be denoted as *coupling fidelity* an exact RMT prediction will be presented below. The coupling constant of the variable perturbing channels will be denoted by λ for $\hat{S}_{ab}(t)$ and λ' for $\hat{S}'^*_{ab}(t)$. Looking at the parametric correlation functions

$\langle \hat{S}_{ab}(t)\hat{S}'^{*}_{ab}(t)\rangle$ in Eq. (2.5) first for the case where $\lambda = \lambda'$, the so called autocorrelation function, and apply the convolution theorem for Fourier transforms we find that it equals the famous Verbaarschot-Weidenmüller-Zirnbauer (VWZ) integral [ver85] and is given by:

$$\langle \hat{S}_{ab}(t)\hat{S}^{*}_{ab}(t)\rangle = \hat{C}[S_{ab}, S^{*}_{ab}](t) = \delta_{ab}T_a^2(1-T_a)J_a(t) + (1+\delta_{ab})T_aT_bP_{ab}(t). \tag{4.7}$$

Here the parametrization of Ref. [gor02] was used to write down the explicit expressions for the functions $J_a(t)$ and $P_{ab}(t)$, as

$$J_a(t) = 4\mathcal{I}\left[\left(\frac{r+T_ax}{1+2T_ar+T_a^2\,x} + \frac{t-r}{1-T_a(t-r)}\right)^2\right] \tag{4.8}$$

and

$$P_{ab}(t) = 2\mathcal{I}\left[\frac{T_aT_bx^2 + d_{ab}(r)x + (2r+1)r}{(1+2T_ar+T_a^2x)(1+2T_br+T_b^2x)} + \frac{(t-r)(r+1-t)}{[1-T_a(t-r)][1-T_b(t-r)]}\right], \tag{4.9}$$

where

$$x \equiv \frac{2r+1}{2u+1}u^2, \quad d_{ab}(r) \equiv T_aT_b + (T_a+T_b)(r+1) - 1$$

and the shorthand $\mathcal{I}$ stands for the integral,

$$\mathcal{I}[\cdots] = \int\limits_{\max(0,t-1)}^{t} \mathrm{d}r \int\limits_{0}^{r} \mathrm{d}u \frac{(t-r)(r+1-t)}{(2u+1)(t^2-r^2+x)^2} \times \prod_{k=1}^{M} \frac{1-T_k(t-r)}{\sqrt{1+2T_kr+T_k^2x}}[\cdots]\,.$$

In this chapter the time t is given in units of the Heisenberg time $t_H = 2\pi\hbar/\Delta$, with Δ being the mean level spacing. For the case of $\lambda \neq \lambda'$ the correlator $\langle \hat{S}_{ab}(t)\hat{S}'^{*}_{ab}(t)\rangle$ has been calculated by D. Savin using supersymmetry techniques (The calculation can be found in the Appendix of [koeb10]). Finally it yields

$$\langle \hat{S}_{ab}(t)\hat{S}'^{*}_{ab}(t)\rangle = \langle \hat{S}^{\mathrm{eff}}_{ab}(t)\hat{S}^{\mathrm{eff}*}_{ab}(t)\rangle. \tag{4.10}$$

This means, that the parametric cross correlation function reduces to an autocorrelation function $\langle \hat{S}^{\mathrm{eff}}_{ab}(t)\hat{S}^{\mathrm{eff}*}_{ab}(t)\rangle$ given by the same VWZ expression (4.7), where the transmission coefficient (Eq. (4.6)) of the varied channel has to be replaced by

$$T^{\mathrm{eff}} = \frac{2\,(\lambda+\lambda'^{*})}{(1+\lambda)\,(1+\lambda'^{*})}\,. \tag{4.11}$$

One can interpret T^{eff} as some effective transmission coefficient due to a parametric variation of the coupling strength in the varied channel. For $\lambda = \lambda'$, the effective transmission coefficient T^{eff} becomes equal to the conventional transmission coefficient (Eq. (4.6)). In contrast to the transmission coefficient in Eq. (4.6) the effective transmission coefficient T^{eff} is generally complex. The subsequent evaluation of the coupling fidelity cannot be done analytically and will be performed numerically.

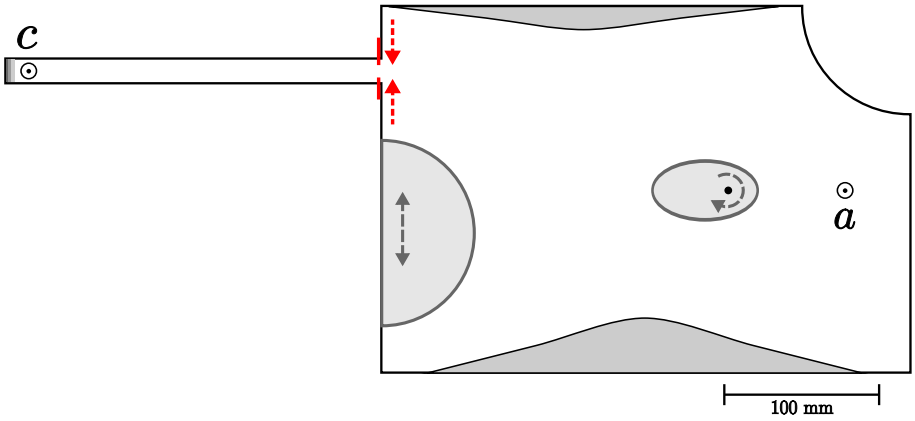

Figure 4.1: Geometry of the chaotic Sinai billiard, length $l = 342\,\text{mm}$, width $w = 237\,\text{mm}$ and a quarter-circle of radius $r = 70\,\text{mm}$, with attached channel of a total length $l_c = 243\,\text{mm}$ and a width $w_c = 16\,\text{mm}$. The opening of the channel can be varied from $d = 0 - 16\,\text{mm}$ in steps of $0.1\,\text{mm}$ using a slit diaphragm. At position a and c two antennas were fixed and connected to the VNA. The additional elements were inserted to reduce the influence of bouncing balls.

4.3 Experiments

Based on a chaotic microwave billiard with attached waveguide, which was used in [per00, stoe02] to study the resonance trapping in an open microwave cavity, we designed our first experiment (SubSec. 4.3.1) for a microwave study of the coupling fidelity. As in this experiment the variation of the coupling was mainly on the real part of the coupling, we introduced a new setup, where predictions of the theory could be varified (see SubSec. 4.3.2).

4.3.1 First experiment: Attached wave guide with variable coupling

Experimental setup

In the first approach the setup shown in Fig. 4.1 was used, where the opening of the variable slit plays the role of the fidelity parameter. The setup is based on a quarter Sinai shaped billiard with length $l = 342\,\text{mm}$, width $w = 237\,\text{mm}$, a quarter-circle of radius $r = 70\,\text{mm}$, and an attached channel. The channel has a total length of $l_c = 243\,\text{mm}$ and a width $w_c = 16\,\text{mm}$. At position a and c two antennas were fixed and connected to the VNA. The complete S-matrix was measured in a frequency range from 9.5 to 18.0 GHz with a resolution of 0.1 MHz, where the wave guide only supports a single propagating mode, i. e. it acts as a single channel. The perturbation of the system was achieved by opening the channel from $d = 0 - 16\,\text{mm}$ in steps of $0.1\,\text{mm}$ using a slit diaphragm at the point of attachment. An ellipse insert with semiaxis $a = 70\,\text{mm}$ and $b = 40\,\text{mm}$ was

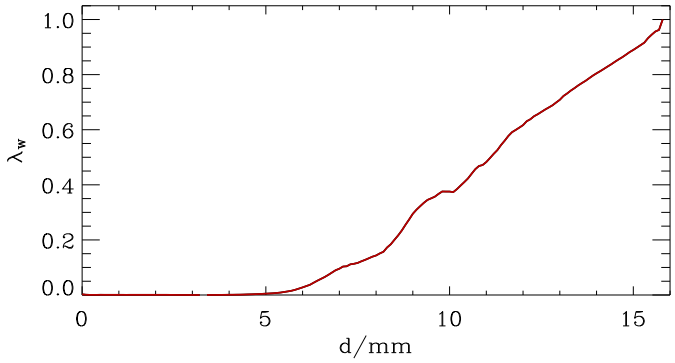

Figure 4.2: λ_W as a function of the opening d, averaged over the frequency window 13 to 14 GHz.

rotated to get an ensemble of 20 different systems for averaging. Additional elements were inserted into the billiard to avoid bouncing-ball resonances. The wave guide was terminated by a perfect absorber, which, according to Eq. (4.22), should correspond to a purely imaginary coupling.

The coupling constant λ_W could be determined directly from a reflection measurement at antenna c using Eq. (4.6). As Fig. 4.2 shows, λ_W can be varied from $\lambda_W = 0$ (no coupling) to $\lambda_W = 1$ (perfect coupling) by increasing the opening d of the slit.

Results and Discussion

In this section we want to discuss the experimental and theoretical results for the coupling fidelity decay under the perturbation described before. For all results below the system with closed slit diaphragm, corresponding to $\lambda = 0$, is chosen as the reference, whereas for the perturbed system the coupling constant is $\lambda' = \lambda_W \neq 0$, depending on the opening d of the slit.

In Fig. 4.3 the coupling fidelity decay is shown for two different perturbation strengths. The filled symbols show the experimental results. With the formulas derived in Sec. 4.2, we calculated the expected theoretical fidelity decay assuming that the channel is totally open, i. e. the coupling is purely imaginary (solid lines). There is obviously no agreement. This shows that something is wrong in the argumentation. For a further check the absorbing end and the antenna in the channel was removed and replaced by a reflecting end thus closing the system. Fig. 4.4 shows, that we did not find any noticeable difference to the case with the absorbing end and the antenna in the channel experimentally. So there is only one explanation: by far the major part of the wave is reflected directly at the slit, and only a minor part really penetrates into the channel!

The solid lines in Fig. 4.5 show the resulting theoretical curves with using an imaginary fitting parameter λ_{fit}. Now a perfect agreement between experiment and theory is

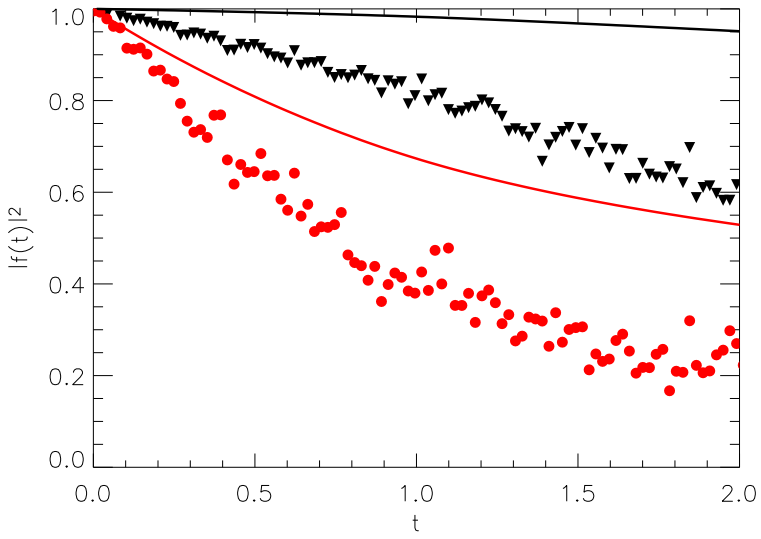

Figure 4.3: Experimental coupling fidelity $|f(t)|^2$ (filled symbols) and theoretical results for the experimental parameter λ_W (solid lines) for two openings $d = 6.5\,\mathrm{mm}$ (black triangles) with $\lambda_W = 0.05$, and $d = 11.2\,\mathrm{mm}$ (red circles) with $\lambda_W = 0.52$. The frequency window of the Fourier transform of the measured $S_{\mathrm{aa}}(\nu)$ was 13 to 14 GHz and the transmission coefficient for antenna a was $T_a = 0.95$.

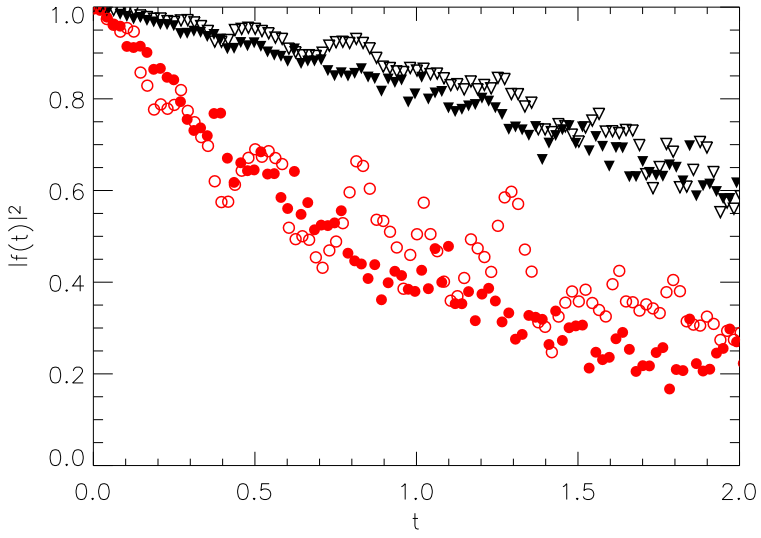

Figure 4.4: Comparison between the experimental coupling fidelity $|f(t)|^2$ results shown in Fig. 4.3 (filled symbols) and results from measurements where the absorbing end and the antenna in the channel have been replaced by a reflecting end thus closing the system (open symbols)

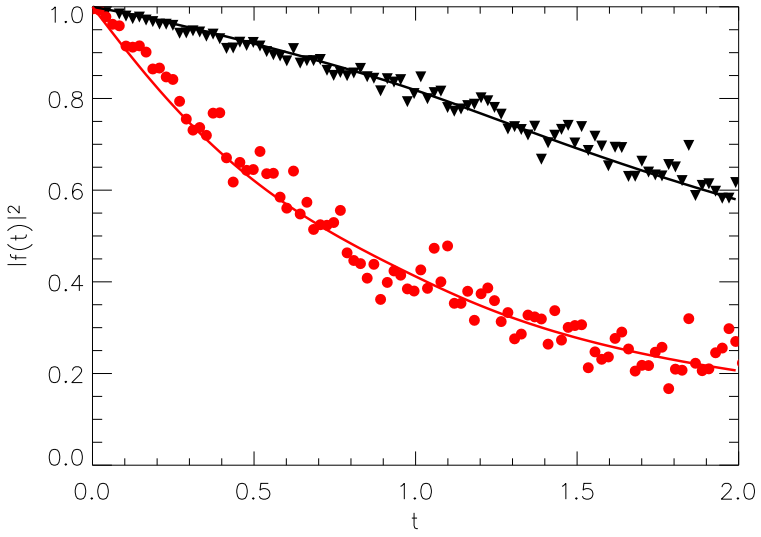

Figure 4.5: Experimental coupling fidelity $|f(t)|^2$ (filled symbols) and theoretical results for the fit parameter λ_{fit} (solid line) for two openings $d = 6.5\,\text{mm}$ (black triangles) with $\lambda_{\text{fit}} = -0.18i$, and $d = 11.2\,\text{mm}$ (red circles) with $\lambda_{\text{fit}} = -0.55i$. The frequency window of the Fourier transform of the measured $S_{\text{aa}}(\nu)$ was 13 to 14 GHz and the transmission coefficient for antenna a was $T_a = 0.95$.

found.

As a resume we can state that a smooth variation of the coupling will not easily yield the information about the effect of coupling to the continuum on the scattering fidelity. Each geometric variation will give rise to both a change of coupling and internal scattering properties, thus screening the purely external effect. Contrary to intuition, for this setup the main effect of the variation of the slit does not correspond to a change of the coupling to the outside, but to a distortion of the wave functions in the billiard, thus corresponding more to the case of a local scattering fidelity [hoeh08, koeb11] as in chapter 3.

The perturbation that results from the wave guide with variable slit and the antenna with absorbing end can not de described as a simple absorption, but there is always a very significant reflecting part. As we have seen we were not able to simply change the perturbation strength by varying the opening of the slit so we decided to go a step back, designing a setup which allows for a separated investigation of perturbations to the scattering fidelity in the case of absorption and reflection (open end and hard wall).

4.3.2 Second experiment: Antenna with different terminators

In our second experiment we remove the wave guide with slit from the experimental setup and inserted a perturbing antenna which was terminated consecutively with three differ-

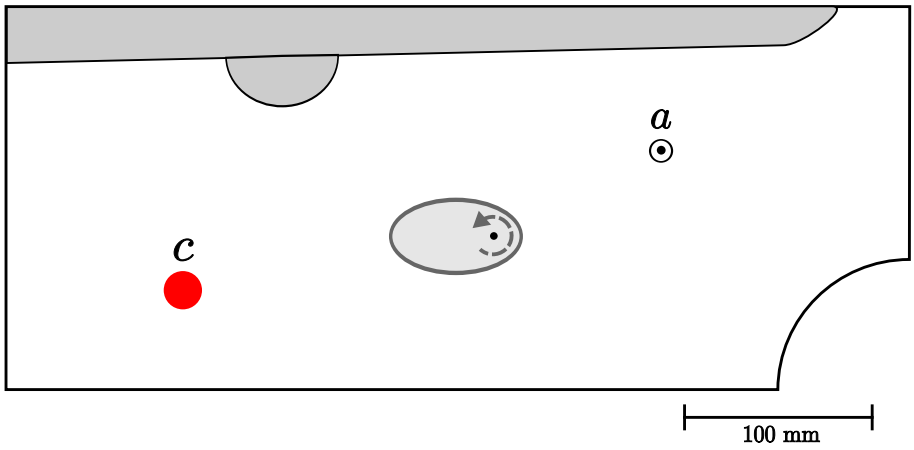

Figure 4.6: Geometry of the chaotic Sinai billiard, length $l = 472\,\mathrm{mm}$, width $w = 200\,\mathrm{mm}$ and a quarter-circle of radius $r = 70\,\mathrm{mm}$ where an antenna with different terminations may be introduced at position c. a denotes the measuring antenna. The additional elements were inserted to reduce the influence of bouncing balls.

ent terminators from a standard calibration kit being part of our microwave equipment. The terminators provide total absorption, open end reflection and hard wall reflection.

Experimental setup

The setup, as illustrated on Fig. 4.6, is again based on a quarter Sinai shaped billiard, where additional elements were inserted into the billiard to reduce the influence of bouncing-ball resonances. So the classical dynamics for the chosen geometry of the billiard is dominantly chaotic. At position a one antenna is fixed and connected to an Agilent 8720ES vector network analyser (VNA), which was used for measurements in a frequency range from 2 to 18 GHz with a resolution of 0.1 MHz. We measured the reflection S-matrix element S_{aa} first for the unperturbed system, which corresponds to the situation, where no additional antenna is inserted at position c. Then we perturbed the system by inserting another antenna at position c which was terminated consecutively in three different ways:

(a) connection to the VNA (total absorption),

(b) standard open (open end reflection),

(c) standard short (hard wall reflection),

and again measured the corresponding reflection at antenna a for each case. The connection of antenna c to the VNA corresponds to a termination of antenna c with a $50\,\Omega$ load. The terminators for the cases (b) and (c) have been taken from the standard calibration kit (Agilent 85052C Precision Calibration Kit) being part of our microwave equipment. For case (a) the reflection amplitude S_{cc} was also measured. From this measurement

the coupling strength of antenna c can be obtained, see Eq. (4.6) above. For all four cases we measured 18 different realizations by rotating an ellipse (see Fig. 4.6) to perform ensemble averages.

The effective Hamiltonian description

In this subsection we present the mapping of the experimental situation onto the more general theoretical description presented in Sec. 4.2 focussing on results and predictions for the three cases of total absorption, open end reflection and hard wall reflection. The calculation is very similar to the approaches that can be found in [stoe02]. To describe our experimental situation we need two scattering channels, the measuring antenna, below denoted by index "a" and the antenna with variable coupling (the perturbing channel) denoted by index "c". The amplitudes of incoming (u) and outgoing (v) waves for this two channels are related via the S-matrix:

$$S \begin{pmatrix} u_c \\ u_a \end{pmatrix} = \begin{pmatrix} v_c \\ v_a \end{pmatrix}. \tag{4.12}$$

For antenna c which is connected with a terminator the connection between the amplitudes u_c and v_c can be described by

$$u_c = r v_c\,, \qquad r = e^{-(\alpha - \imath\varphi)}\,, \tag{4.13}$$

where r contains the information on the reflection properties of the antenna. For reflection at an antenna with open end (index "oe") or hard wall (index "hw") we have no absorption $\alpha = 0$ as long as the absorption in the antenna can be neglected and a difference in total phase shift $\varphi_{\mathrm{oe}} - \varphi_{\mathrm{hw}} = \pi$. The termination of the antenna by a $50\,\Omega$ load corresponding to total absorption is given by $\alpha \to \infty$.

With the expression of the scattering matrix in terms of Wigner's reaction matrix:

$$S = \frac{1 - iW^\dagger G W}{1 + iW^\dagger G W}\,. \tag{4.14}$$

$G = (E - H)^{-1}$ is the Green function of the closed system and matrix $W = (W_a, W_c)$ contains the information on the coupling, one can rewrite (4.12) as

$$iW^\dagger G W \begin{pmatrix} u_c + v_c \\ u_a + v_a \end{pmatrix} = \begin{pmatrix} u_c - v_c \\ u_a - v_a \end{pmatrix}. \tag{4.15}$$

Substituting relation (4.13) in Eq. (4.15) one can eliminate u_c and v_c and end up with an equation for u_a and v_a,

$$iW_a^\dagger \hat{G} W_a (u_a + v_a) = u_a - v_a. \tag{4.16}$$

In this equation, we have introduced the modified Green function $\hat{G}$, with the following matrix element

$$W_a^\dagger \hat{G} W_a \equiv G_{aa} - G_{ac} \frac{1}{1 + i\lambda_T G_{cc}} i\lambda_T G_{ca}\,, \tag{4.17}$$

where $G_{nm} = W_n^\dagger G W_m$ and λ_T is the coupling constant of the "terminator",

$$\lambda_T = \frac{1-r}{1+r} = \tanh\frac{\alpha + i\varphi}{2}\,. \tag{4.18}$$

Eq. (4.15) is the reduced form of Eq. (4.16) for the measuring antenna, where the variational antenna is accounted for in the modified Green function $\hat{G}$. Using the explicit expressions for matrix elements G_{nm}, we obtain in a number of elementary steps

$$\begin{aligned}
\hat{G} &= G - GW_c \frac{1}{1 + i\lambda_T W_c^\dagger G W_c} i\lambda_T W_c^\dagger G \\
&= G\left[1 - \frac{1}{1 + i\lambda_T W_c W_c^\dagger G} i\lambda_T W_c W_c^\dagger G\right] \\
&= G\frac{1}{1 + i\lambda_T W_c W_c^\dagger G} \\
&= \frac{1}{E - H^a_{\text{eff}}}\,,
\end{aligned} \tag{4.19}$$

where $H^a_{\text{eff}} = H - i\lambda_T W_c W_c^\dagger$. We can rewrite this expression, introducing the normalized coupling vector $V = \frac{1}{\sqrt{\lambda_W}} W_c$, where $\lambda_W = W_c^\dagger W_c$ is the channel coupling strength, as

$$H^a_{\text{eff}} = H - i\lambda V V^\dagger, \quad \lambda = \lambda_T \lambda_W\,. \tag{4.20}$$

The quantity λ is the total coupling constant, which is generally complex and takes into account the effects of both the channel coupling (λ_W) and the terminator (λ_T). To remind you λ is our perturbation parameter for the coupling fidelity. Having a look at the S-Matrix we find, that the 2×2 scattering matrix (Eq. (4.14)) for the measuring antenna and the antenna with variable terminator has thus been reduced to a 1×1 scattering matrix for the measuring antenna only,

$$S_{aa} = \frac{1 - iW_a^\dagger \frac{1}{E - H^a_{\text{eff}}} W_a}{1 + iW_a^\dagger \frac{1}{E - H^a_{\text{eff}}} W_a}. \tag{4.21}$$

This bottom up result can be directly connected to top down result of Eq. (4.4). Because in case of a single measurement antenna and one antenna with variable coupling, Eq. (4.21) is equivalent to Eq. (4.4). In Eqs. (4.20) and (4.21) the main result of this section are written down. They show that the influence of the variable antenna can be taken into account by an appropriate modification of the Hamiltonian.

Now we focus on the special cases which are not only of particular importance for our experimental situation. In the case where the outgoing wave is completely absorbed (here the termination of the antenna is realized with a $50\,\Omega$ load) the corresponding limit is $\alpha \to \infty$ as already mentioned. For this case it follows that $\lambda_T = \tanh\infty = 1$ and

$$H^a_{\text{eff}} = H - i\lambda_W V V^\dagger\,. \tag{4.22}$$

So the coupling is purely imaginary.

For the two cases, where the antenna is terminated by a reflecting hard wall or an open end, we may assume $\alpha = 0$, resulting in $\lambda_T = \tanh(i\varphi/2) = i \tan \varphi/2$, and

$$H^a_{\text{eff}} = H + \tan\left(\frac{\varphi}{2}\right) \lambda_W V V^\dagger \,. \tag{4.23}$$

Here the coupling is purely real and the antenna does not correspond any longer to an open channel but only to a scattering centre. In fact this interpretation is true only as long as the absorption in the antenna can really be neglected. It becomes questionable, as soon as φ approaches π, corresponding to the excitation of a resonance within the antenna. For this singular situation the perturbative treatment of the antenna coupling applied in the derivation looses its justification. The value of the total phase shift φ depends on the length of the antenna in units of the wave length and thus on frequency ν. But independently of frequency the difference of the phase shift φ for the reflection at the open end (oe) and the hard wall (hw), respectively, is always π, as already mentioned. A phase difference of π means a replacement of the tangent by the cotangent in Eq. (4.23), i. e. the coupling constants λ_T for the two situations are related via

$$\lambda_{T,\text{hw}} \lambda_{T,\text{oe}} = 1 \tag{4.24}$$

With the above introduced total coupling constant $\lambda = \lambda_T \lambda_W$ this may be alternatively written as

$$\lambda_{\text{hw}} \lambda_{\text{oe}} = \lambda_W^2 = \lambda_{50\Omega}^2 \tag{4.25}$$

since λ_W is the coupling constant for the $50\,\Omega$ load (see Eq. (4.22)). λ_{hw} and λ_{oe} denote the total coupling constants for the hard-wall and the open-end reflections. These relations allow for explicit tests of the theory.

Results and Discussion

In this section we want to discuss the experimental and theoretical results for the coupling fidelity decay under the perturbations (a)-(c) described in Sec. 4.3.2. For all results below the system without the varied antenna, corresponding to $\lambda = 0$, is chosen as the reference, whereas for the perturbed system the coupling parameter is $\lambda' = \lambda_{50\Omega}$, λ_{oe}, or λ_{hw}, depending on the terminator.

Before the fidelity results will be presented we want to look at the transmission coefficients because this quantity gives first information on the coupling of the two antenna a and c and is determined directly from the measured reflection matrix elements via Eq. (4.6). In Fig. 4.7 the transmission coefficients T_a and T_c are plotted as a function of the mean frequency ν, averaged over a frequency window of 1 GHz. The values of the transmission coefficients change as a function of frequency. This gave us the possibility to vary the coupling strength of our perturbing antenna c by choosing certain frequency windows. The corresponding coupling constant λ_W of antenna c which can be calculated directly from the transmission coefficient T_c (Eq. (4.2)) is plotted in Fig. 4.8.

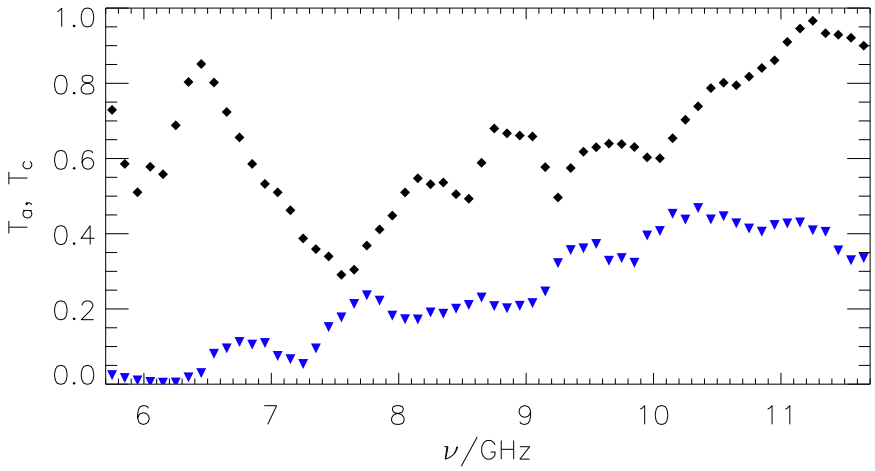

Figure 4.7: Transmission coefficient T_a (triangles; blue) and T_c (diamonds; black) as a function of the mean frequency ν, averaged over a frequency window of 1 GHz.

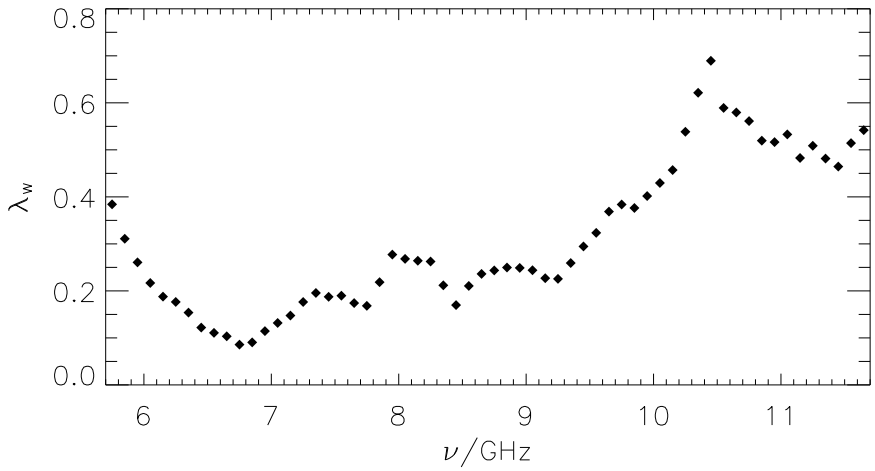

Figure 4.8: Coupling constant λ_W as a function of the mean frequency ν, averaged over the frequency window width of 1 GHz. Determined from the Transmission coefficient T_c.

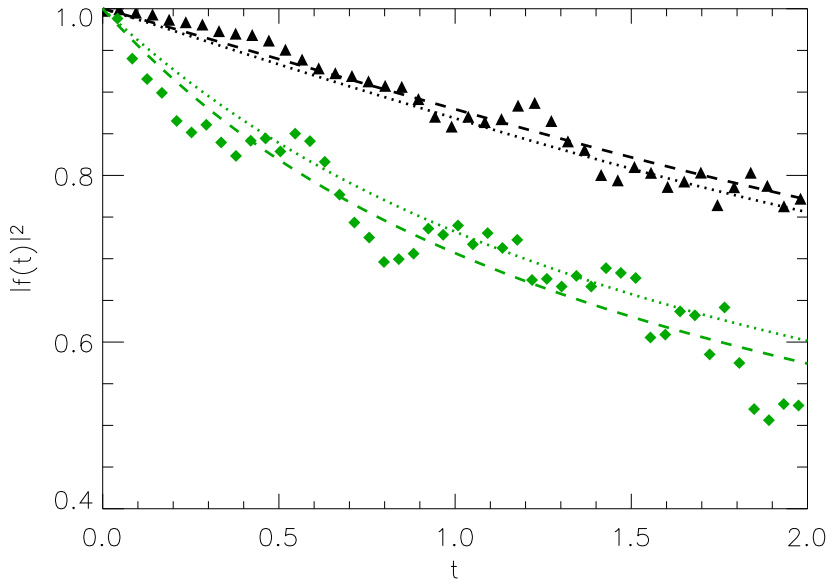

Figure 4.9: Fidelity decay $|f(t)|^2$ for perturbation $\lambda_{50\Omega}$. Filled symbols show the experimental results and the theoretical curves are dotted for experimental parameter and dashed for fitting parameter. Chosen frequency ranges: $8.7-9.2\,\mathrm{GHz}$ (black triangles) with $\lambda_{50\Omega}^{\mathrm{expt}} = 0.24$, $\lambda_{50\Omega}^{\mathrm{fit}} = 0.21$ and $9.8-10.3\,\mathrm{GHz}$ (green diamonds) with $\lambda_{50\Omega}^{\mathrm{expt}} = 0.43$, $\lambda_{50\Omega}^{\mathrm{fit}} = 0.46$.

Antenna with 50 Ω load We start the presentation and discussion of our fidelity results with the case of perturbation (a) (total absorption). According to Eq. (4.22) we expect a purely imaginary coupling with $\lambda_{50\Omega} = \lambda_W$. In Fig. 4.9 the fidelity introduced in Eq. (2.6) is plotted for two frequency ranges corresponding to two different coupling strengths λ_W. Using the experimentally determined λ_W here denoted as coupling parameter $\lambda_{50\Omega}^{\mathrm{expt}}$, one gets already a very good agreement between experimental results (filled symbols) and theoretical curves (dotted line) without any fit. A fit of λ_W to the experimental curves (the corresponding values are denoted by $\lambda_{50\Omega}^{\mathrm{fit}}$) which is plotted as dashed line shows only a minor improvement for the correspondence between experiment and theory.

As a second example in Fig. 4.10 we present the fidelity decay for the frequency range $7.2-7.7\,\mathrm{GHz}$. Here we find a obvious deviation between the experimental results (filled circles) and the theoretical curve based on the experimental parameter $\lambda_{50\Omega}^{\mathrm{expt}}$ (dotted line). To determine the decay of the experimental fidelity decay we tried two possible ways of fitting λ_W to the experimental data. The first way uses a real valued fitting parameter $\lambda_{50\Omega}^{\mathrm{fit,re}}$ (black dashed line) while in the second way to experimental parameter $\lambda_{50\Omega}^{\mathrm{expt}}$ an imaginary part is added as fitting parameter, coming up with a complex valued $\lambda_{50\Omega}^{\mathrm{fit,im}}$.

While for the fidelity decays both fitting procedure lead to a good agreement between experiment and theory, the corresponding fidelity amplitude presented in Fig. 4.11 (on the right side) is described satisfying in real $f_R(t)$ and imaginary part $f_I(t)$ only by the

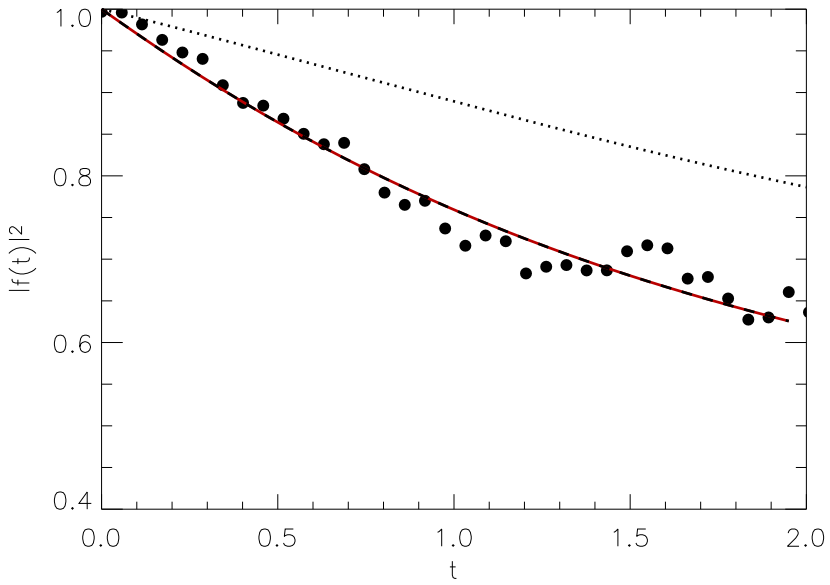

Figure 4.10: Fidelity decay $|f(t)|^2$ for perturbation $\lambda_{50\Omega}$ in frequency range 7.2−7.7 GHz. Filled circles show the experimental results. The theoretical curves are dotted for experimental parameter $\lambda_{50\Omega}^{\text{expt}} = 0.19$; dashed black for real valued fitting parameter $\lambda_{50\Omega}^{\text{fit,re}} = 0.37$ and dashed red for complex valued fitting parameter $\lambda_{50\Omega}^{\text{fit,im}} = 0.19 + i0.20$.

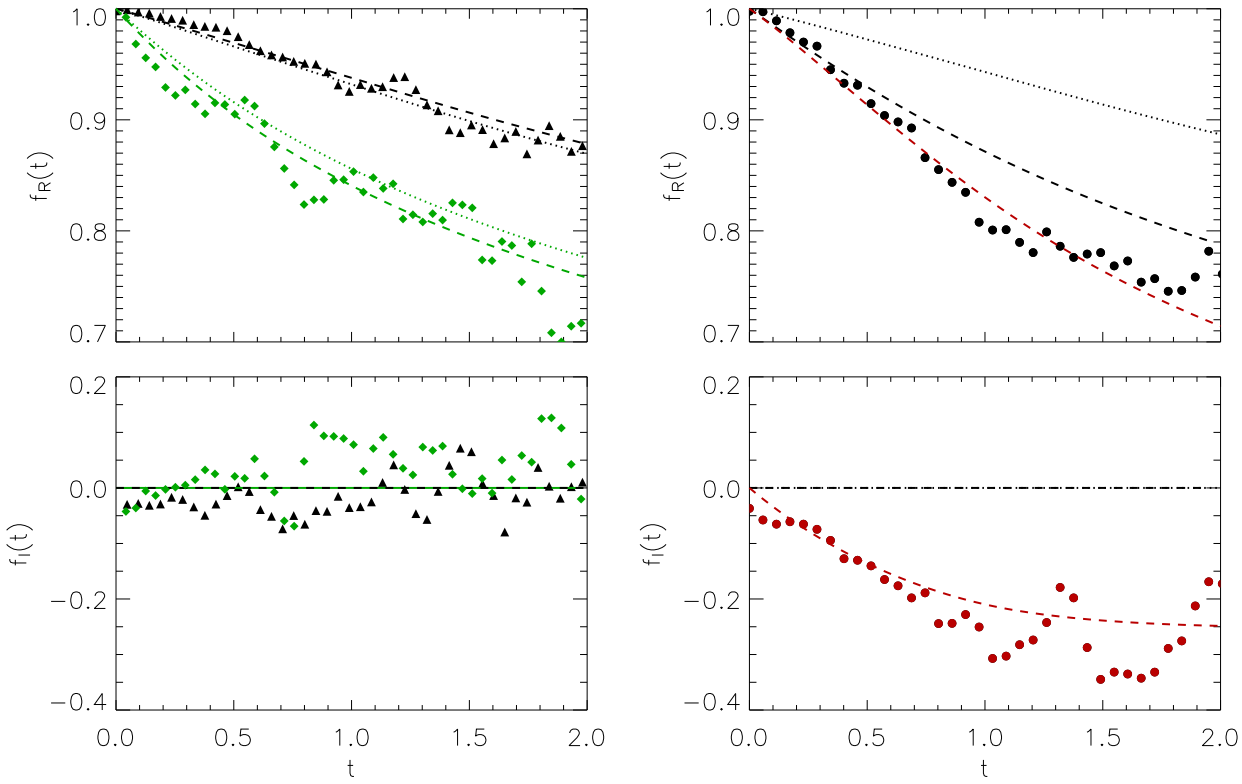

Figure 4.11: Real part $f_R(t)$ and imaginary part $f_I(t)$ of the fidelity amplitude for perturbation $\lambda_{50\Omega}$. The two plots on the left correspond to the two cases presented in Fig. 4.9 and the two plots on the right correspond to the cases presented in Fig. 4.10

red dashed curve, which is generated with the complex valued fitting parameter $\lambda_{50\Omega}^{\mathrm{fit,im}}$. In the case of total absorption one would expect the imaginary part of the fidelity amplitude ($f_I(t)$) to be zero because the correlation function Eq. (4.10) is real valued as long as the coupling parameters λ entering via Eq. (4.11) are real. For the plot on the left side in Fig. 4.11 the experimental results show only a small deviation from the theoretical expected zero in the imaginary part of the fidelity amplitude. The significant imaginary part in the experimental fidelity amplitude for the case of frequency range $7.2 - 7.7\,\mathrm{GHz}$ means that in this frequency range the $50\,\Omega$ terminator does not correspond to perfect absorption, and Eq. (4.23) does not hold. This might be due to an antenna resonance, leading to an increased reflection from the channel c.

In Fig. 4.12 we plotted the coupling constant λ_W determined from the experimental Transmission coefficient T_c as $\lambda_{50\Omega}^{\mathrm{expt}}$ (black triangles) and from the fit to the experimental fidelity decay $\lambda_{50\Omega}^{\mathrm{fit,re}}$ (red diamonds). For frequencies from about 6 GHz up to 10 GHz the experimental determined coupling constant and the fitting parameter does not deviate to much from each other apart from some significant peaks like the one around 7.5 GHz which results from system specific features, probably antenna resonances. Be-

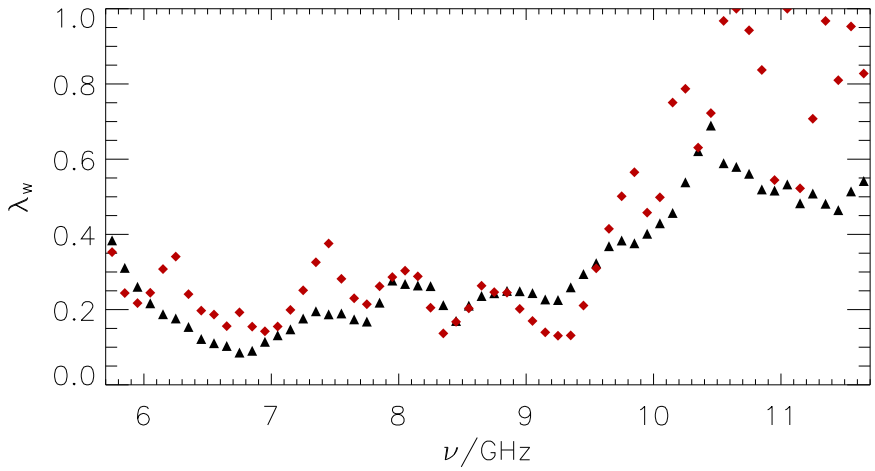

Figure 4.12: Coupling constant λ_W as a function of the mean frequency ν; determined from the experimental Transmission coefficient T_c (black triangles) and as real valued fitting parameter to the experimental fidelity decay (red diamonds).

	ν/GHz	$\lambda^{\text{exp}}_{50\Omega}$	$\lambda^{\text{fit}}_{50\Omega}$	λ_{oe}	λ_{hw}	$\sqrt{\lambda_{\text{oe}}\lambda_{\text{hw}}}$
(i)	$7.2-7.7$	0.19	0.37	$0.65\,\imath$	$-0.04\,\imath$	0.16
(ii)	$8.0-8.5$	0.21	0.20	$0.19\,\imath$	$-0.23\,\imath$	0.21
(iii)	$8.7-9.2$	0.24	0.21	$0.05\,\imath$	$-0.83\,\imath$	0.20

Table 4.1: Coupling constants in the three different frequency ranges (i)-(iii). According to Eq. (4.25), $\lambda^{\text{exp}}_{50\Omega}$ and $\lambda^{\text{fit}}_{50\Omega}$ should be compared to $\lambda_W = \sqrt{\lambda_{\text{oe}}\lambda_{\text{hw}}}$, see Fig. 4.13 and main text for discussion.

yond 11 GHz the way of determing the coupling constant via a reflection measurement at the perturbing antenna c does not lead to convincing results. This might be due to the resonance trapping effect which was observed in microwave billiards in [per00], but is not examined so far.

Antenna with reflecting end In Fig. 4.13 we present the experimental and theoretical fidelity results for the situations open end (blue) and hard wall reflection (red) as perturbation, for three frequency ranges. For each frequency range we plotted the fidelity $|f(t)|^2$ (large figures left) and the corresponding fidelity amplitude as real $f_R(t)$ and imaginary part $f_I(t)$ (small figures right). We want to remind you, that for the correct description for this situations, where the systems are closed, is given by Eq. (4.23). In case of closed channels the total phase shift φ increases monotonically with frequency. Thus λ_{oe} and λ_{hw} are oscillating in counter phase. This induces a corresponding oscillation in the strength of the fidelity decay, which can be nicely seen in Fig. 4.13(i)-(iii) for the plots of $|f(t)|^2$ and $f_R(t)$ but also or the imaginary part $f_I(t)$ of the fidelity amplitude.

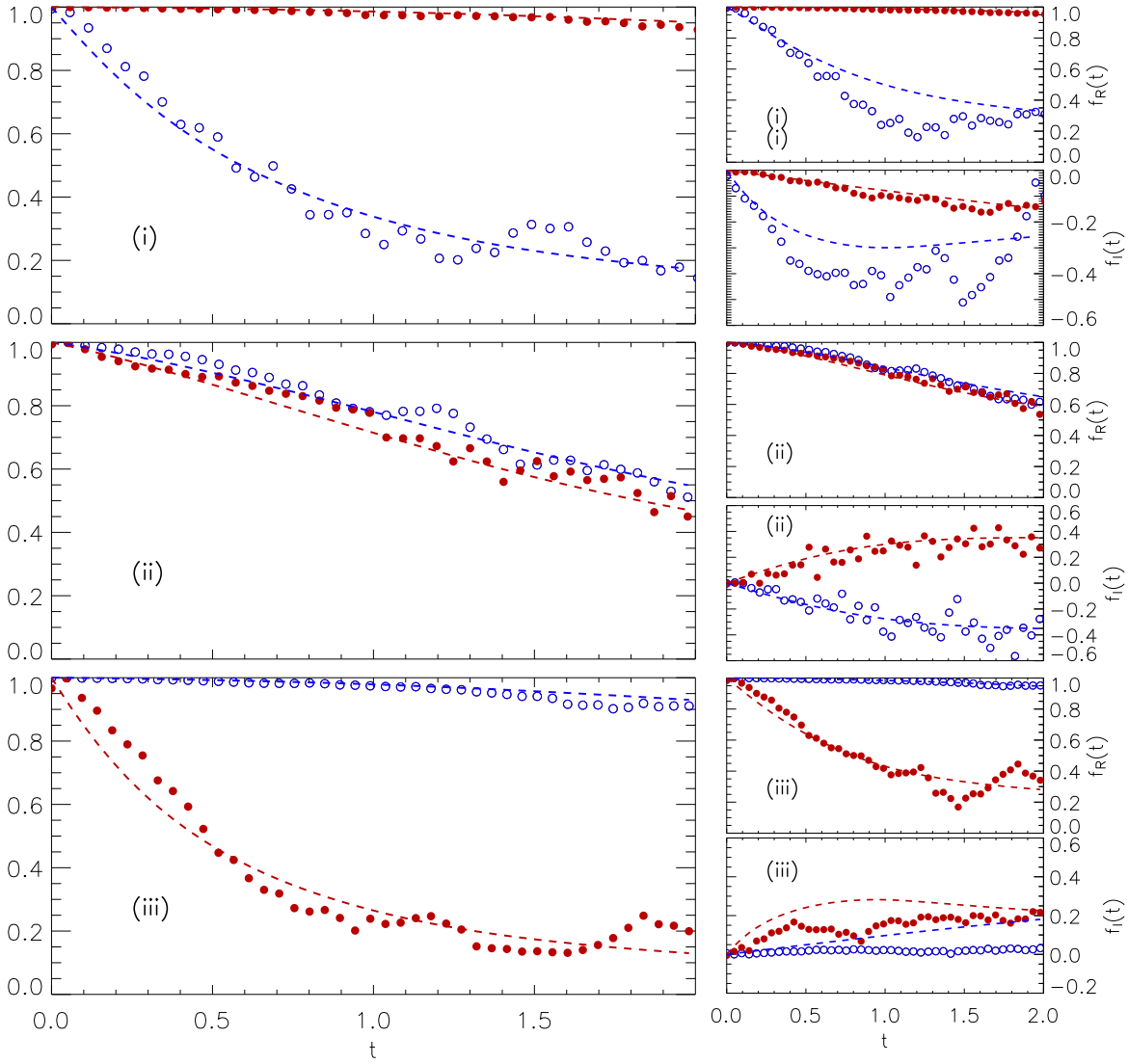

Figure 4.13: Fidelity decay $|f(t)|^2$ and corresponding fidelity amplitude ($f_R(t)$ and $f_I(t)$) for perturbations λ_{hw} (red) and λ_{oe} (blue) in three different frequency ranges: (i) $7.2 - 7.7\,\mathrm{GHz}$; (ii) $8.0 - 8.5\,\mathrm{GHz}$; (iii) $8.7 - 9.2\,\mathrm{GHz}$. The experimental results are depicted by filled (λ_{hw}) and open (λ_{oe}) circles and the dashed curves show the theoretical results. The values of corresponding coupling parameter are listed in Tab. 4.1.

For a more quantitative discussion we compare the experimentally determined fidelity decay (solid lines) to the theoretical curves (dashed lines). The theoretical curves are all results from a fit to the experimental data for the fidelity decay $|f(t)|^2$, the resulting parameter are used to plot the fidelity amplitude, so there is no second fitting for the experimental data in the real $f_R(t)$ and imaginary part $f_I(t)$. In Fig. 4.13 one sees that fitting the experimental results works well for $|f(t)|^2$ in all three frequency ranges. Using this free fitting parameter for $f_R(t)$ also leads to a satisfying agreement, apart from smaller deviations in the case of open end reflection in Fig. 4.13(i). The agreement between experiment and theory is also satisfying for the imaginary part $f_I(t)$ of open end and hard wall reflection in Fig. 4.13(ii) and in the case of open end reflection in Fig. 4.13(i). Only in Fig. 4.13(iii) and again for the case of open end reflection in Fig. 4.13(i) we see some deviations for $f_I(t)$. This is not that surprising because by calculating $|f(t)|^2$ from the real an imaginary part of the fidelity amplitude we lose information, so we could not expect perfect agreement while using the fitting parameter for the real and imaginary part of fidelity amplitude, but the general tendency is always shown by the dashed lines.

We also presented the fidelity amplitude to show that as one would expect from theory [1] for the case of reflecting ends one see a significant imaginary part of the fidelity amplitude $f_I(t)$. Additionally in Fig. 4.13(ii) one can see that whenever the real part $f_R(t)$ of the fidelity amplitude are nearly equal, the imaginary part $f_I(t)$ due to the difference in phase shift between hard wall and open end reflection shows nearly a symmetric behaviour according to the horizontal axis.

Having discussed three frequency ranges exemplary, we now look at the coupling parameter for the two cases of reflecting ends as a function of the frequency. From the fitting parameters λ_{hw} and λ_{oe} we determined the corresponding λ_T dividing out $\lambda_W = \lambda_{50\Omega}^{\mathrm{expt}}$ and finally calculated the total phase shift φ using relations presented in Eq. (4.23). The parameter $i\lambda$, $i\lambda_T$, φ and their absolute values are plotted in Fig. 4.14. The series of plots on the right hand side gives a illustration of the oscillation in the fidelity. Over a frequency range of $\approx 6\,\mathrm{GHz}$ and we see a full and a half period of oscillations. As expected the total phase shift $\varphi \bmod 2\pi$ in the left plot at the bottom shows a satisfying linear increasing with frequency which is more convincing in the frequency range between 7 and 9 GHz. This fact can also be seen in the top plot of Fig. 4.15 where the resulting difference in total phase shift $\Delta\varphi$ between the hard wall and open end reflection is shown for the same frequencies. The expected phase shift $\Delta\varphi = \pi$ plotted as solid horizontal line is only achieved in the mentioned frequency range.

Finally we perform checks on the coupling constants based on Eq. (4.24) and (4.25). A first check on the the coupling constants λ_T based on Eq. (4.24) (bottom plotted in Fig. 4.15) shows that the expected value of one (solid line) is again achieved in the frequency range between 7 and 9 GHz. So we can state that we have confirmed experimentally the theoretical prediction for the fidelity in the case of perturbation by an antenna with reflecting ends for this frequency regime.

[1] In theory the correlation function Eq. (4.10) is complex valued as long as the coupling parameters λ entering via Eq. (4.11) are complex.

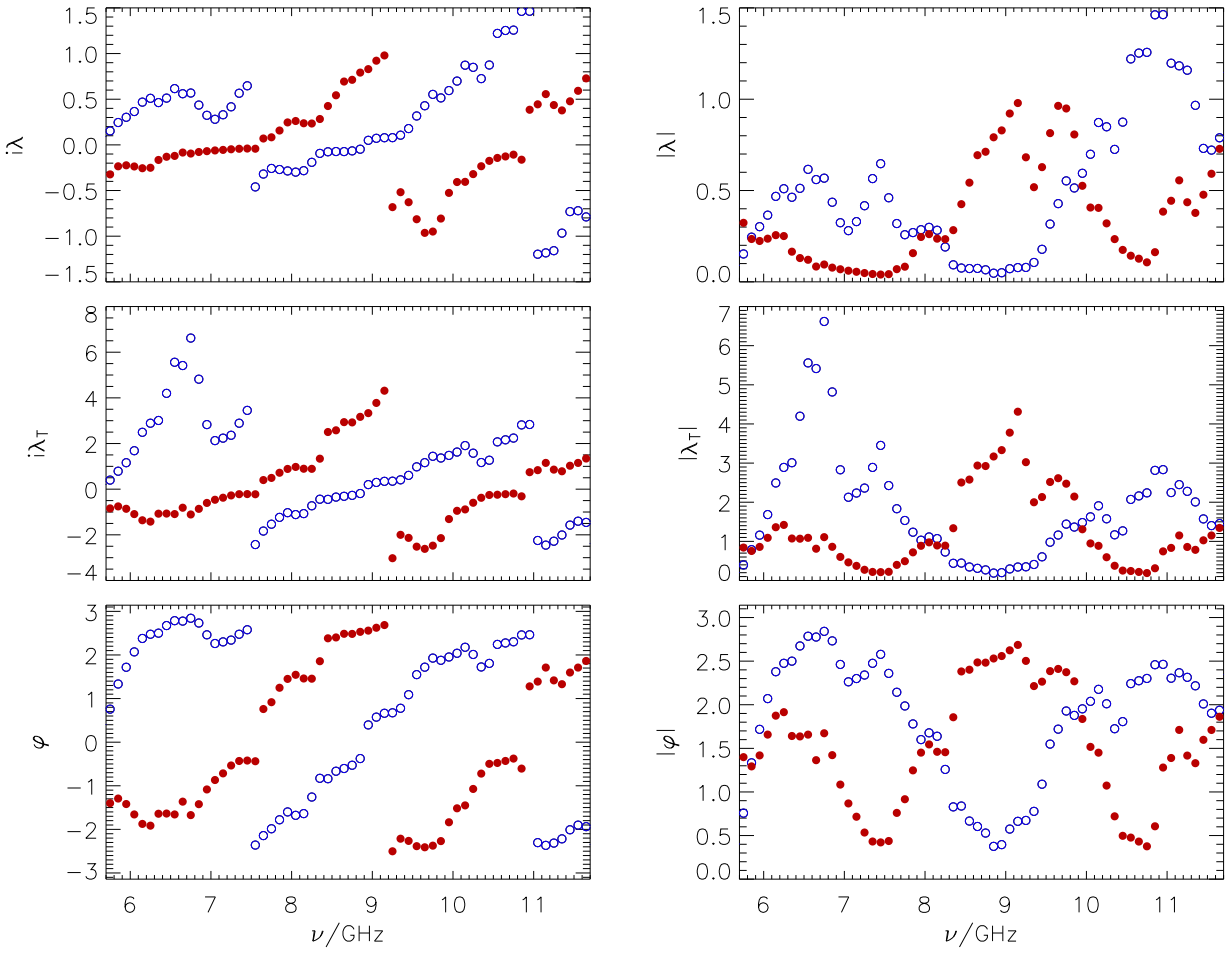

Figure 4.14: Parameters for the two cases of reflecting ends: λ_{hw} (red filled circles) and λ_{oe} (blue open circles) as a function of mean frequency ν. The three pictures on the left show the imaginary part $i\lambda$ of the total coupling parameter (top), the imaginary part $i\lambda_T$ of the coupling constant of the terminators (middle) and the phase shift φ mod 2π (bottom). The pictures on the right show the corresponding absolute values

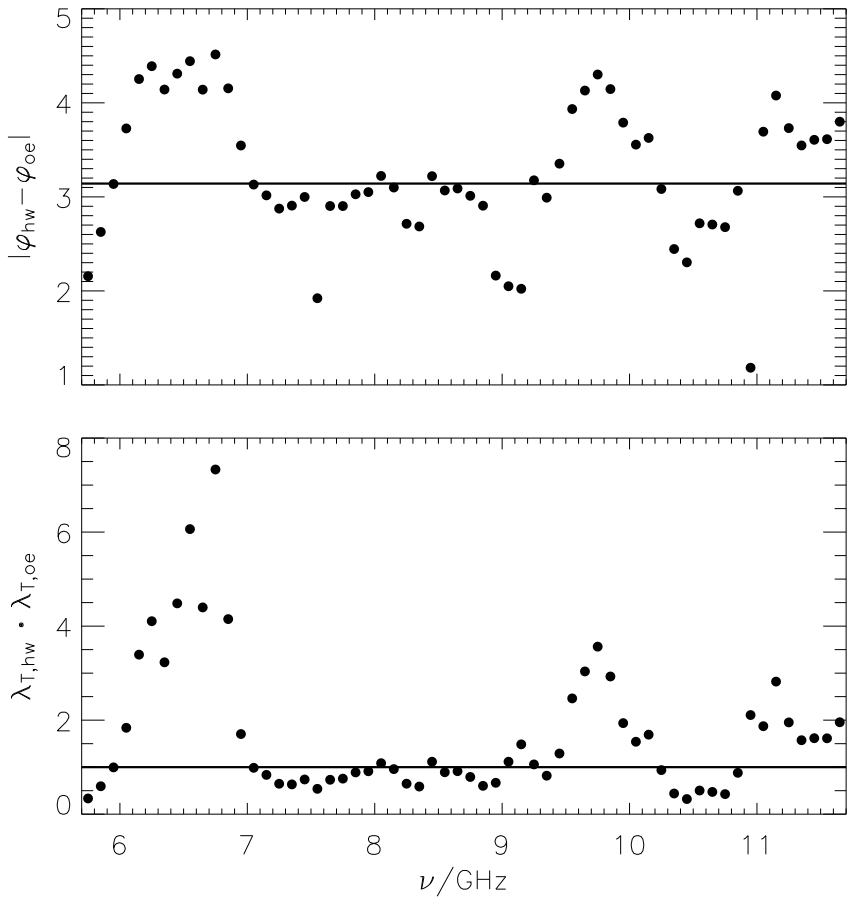

Figure 4.15: Difference of the phase shift φ between the hard wall and open end reflection (top) and the relation between $\lambda_{T,\mathrm{hw}}$ and $\lambda_{T,\mathrm{oe}}$ presented in Eq. 4.24 (bottom) as a function of the mean frequency ν.

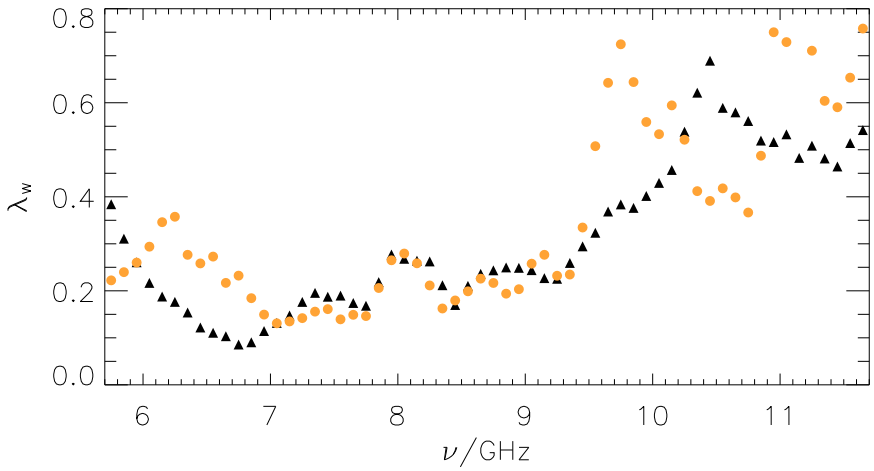

Figure 4.16: coupling constant λ_W as a function of the mean frequency ν; determined from the experimental Transmission coefficient T_c (black triangles) and as $\lambda_W = \sqrt{\lambda_{\mathrm{oe}}\lambda_{\mathrm{hw}}}$ (see Eq. 4.25) (orange filled circles)

Check of the relation between the three terminations According to Eq. (4.25), the square root of the product of the coupling constants for open end and hard wall reflection should give λ_W. Table 4.1 shows that for the frequency ranges (ii) and (iii) there is indeed a good agreement between $\sqrt{\lambda_{\mathrm{oe}}\lambda_{\mathrm{hw}}}$, $\lambda^{\mathrm{fit}}_{50\Omega}$ and $\lambda^{\mathrm{exp}}_{50\Omega}$. In the case (i) $\sqrt{\lambda_{\mathrm{oe}}\lambda_{\mathrm{hw}}}$ agrees quite good with the experimental parameter $\lambda^{\mathrm{exp}}_{50\Omega}$, but the fitting parameter is much larger. This deviation reconfirms our arguments presented in the above discussion in paragraph: Antenna with 50 Ω load.

Again extending our considerations looking at $\sqrt{\lambda_{\mathrm{oe}}\lambda_{\mathrm{hw}}}$ as a function of frequency and compare this quantity with $\lambda^{\mathrm{exp}}_{50\Omega}$. Plotting the two ways of determine the coupling constant λ_W in Fig. 4.16 again shows a good agreement in the whole frequency range between 7 and 9 GHz. So we checked the consistency of the theory for this regime. The reasons for this experimental limits have not been examined so far.

5 Conclusion

In this thesis I presented two works on scattering fidelity decay in a chaotic microwave billiard. The first work describes the first experimental verification of the semiclassical predictions for fidelity decay arising from a local boundary perturbation of a chaotic quantum system and the second work, the influence of the coupling to the continuum on the decay of fidelity was examined experimentally. This studies complements previous experiments of our group, where the fidelity decay under the influence of various types of geometrical perturbations was studied [sch05a, hoeh08, sch05b, bod09] but for closed systems exclusively.

In particular in the first work, we could confirm that the rate governing exponential fidelity decay exhibits oscillations as a function of the perturbation strength. The observed non-monotonic behavior implies that for certain ranges of the perturbation strength the fidelity decay becomes weaker (for fixed time) with increasing perturbation strength. While the original semiclassical treatment [gou08] for a piston-type local boundary deformation was based on the assumption of a small piston displacement, the present microwave setting required a generalization of the semiclassical approach to arbitrary ratios between piston displacement and width, which was performed by deriving an expression for the decay exponent in terms of a quadrature in [koeb11]. Quantitative agreement between the measurements and this refined semiclassical theory was found despite the fact that the microwave billiard does not really satisfy the underlying semiclassical assumption, namely that the extent of the local perturbation, here the piston width w, should be much larger than the de Broglie wave length λ. On experimental side, there remains the challenge to observe fidelity decay in the escape rate regime (for strong perturbations) characterized by a perturbation-independent fidelity decay rate. Naturally, this regime is difficult to access since the expected signals are tiny.

In the second work we could confirm the prediction for the coupling fidelity in terms of a modified VWZ (Verbaarschot, Weidenmüller, Zirnbauer) integral [koeb10] experimentally. First we found, that a smooth variation of the coupling, e. g. by varying the coupling to an attached wave guide will not easily yield the information about the effect of coupling to the continuum on the scattering fidelity. Each geometric variation will give rise to both a change of coupling and internal scattering properties, thus screening the purely external effect, as discussed in Sec. 4.3.1. Secondly, we have included closed channels within the description of VWZ. The speed of the fidelity decay for the open end and hard wall reflection oscillates with frequency due to the corresponding variation of the phase with frequency. A relation connecting the coupling parameters for the closed channel (λ_{oe}, λ_{hw}) to those of the open channel ($\lambda_{50\Omega}$) has been verified experimentally. In all cases the fidelity decay for at least one of the reflecting antennas is faster than for

the open channel, showing the strong influence of the imaginary part on the coupling constant λ.

Bibliography

[alt97] H. Alt, C. Dembowski, H.-D. Gräf, R. Hofferbert, H. Rehfeld, A. Richter, R. Schuhmann, and T. Weiland. Wave dynamical chaos in a superconducting three-dimensional Sinai billiard. *Phys. Rev. Lett.* **79**, 1026 (1997).

[are09] N. Ares and D. A. Wisniacki. Loschmidt echo and the local density of states. *Phys. Rev. E* **80**, 046216 (2009).

[ber87] M. V. Berry. The Bakerian lecture, 1987: Quantum chaology. *Proc. R. Soc. Lond. A* **413**, 183 (1987).

[blue92] R. Blümel, I. H. Davidson, W. P. Reinhardt, H. Lin, and M. Sharnoff. Quasi-linear ridge structures in water surface waves. *Phys. Rev. A* **45**, 2641 (1992).

[bod09] J. D. Bodyfelt, M. C. Zheng, T. Kottos, U. Kuhl, and H.-J. Stöckmann. Probing localization in absorbing systems via Loschmidt echos. *Phys. Rev. Lett.* **102**, 253901 (2009).

[bog06] E. Bogomolny, B. Dietz, T. Friedrich, M. Miski-Oglu, A. Richter, F. Schäfer, and C. Schmit. First experimental observation of superscars in a pseudointegrable barrier billiard. *Phys. Rev. Lett.* **97**, 254102 (2006).

[cer02] N. R. Cerruti and S. Tomsovic. Sensitivity of wave field evolution and manifold stability in chaotic systems. *Phys. Rev. Lett.* **88**, 054103 (2002).

[cuc02] F. M. Cucchietti, C. H. Lewenkopf, E. R. Mucciolo, H. M. Pastawski, and R. O. Vallejos. Measuring the Lyapunov exponent using quantum mechanics. *Phys. Rev. E* **65**, 046209 (2002).

[dit00] F.-M. Dittes. The decay of quantum systems with a small number of open channels. *Phys. Rep.* **339**, 215 (2000).

[doer98] U. Dörr, H.-J. Stöckmann, M. Barth, and U. Kuhl. Scarred and chaotic field distributions in three-dimensional Sinai-microwave resonators. *Phys. Rev. Lett.* **80**, 1030 (1998).

[ell95] C. Ellegaard, T. Guhr, K. Lindemann, H. Q. Lorensen, J. Nygård, and M. Oxborrow. Spectral statistics of acoustic resonances in aluminium blocks. *Phys. Rev. Lett.* **75**, 1546 (1995).

[fyo05] Y. V. Fyodorov, D. V. Savin, and H.-J. Sommers. Scattering, reflection and impedance of waves in chaotic and disordered systems with absorption. *J. Phys. A* **38**, 10731 (2005).

[fyo97] Y. V. Fyodorov and H.-J. Sommers. Statistics of resonance poles, phase shifts and time delays in quantum chaotic scattering: Random matrix approach for systems with broken time-reversal invariance. *J. Math. Phys.* **38**, 1918 (1997).

[gor02] T. Gorin and T. H. Seligman. Signatures of the correlation hole in total and partial cross sections. *Phys. Rev. E* **65**, 026214 (2002).

[gor06] T. Gorin, T. H. Seligman, and R. L. Weaver. Scattering fidelity in elastodynamics. *Phys. Rev. E* **73**, 015202(R) (2006).

[gou07] A. Goussev and K. Richter. Loschmidt-echo decay from local boundary perturbations. *Phys. Rev. E* **75**, 015201(R) (2007).

[gou08] A. Goussev, D. Waltner, K. Richter, and R. A. Jalabert. Loschmidt echo for local perturbations: non-monotonic cross-over from the Fermi-golden-rule to the escape-rate regime. *New J. of Physics* **10**, 093010 (2008).

[gut07] M. Gutzwiller. Quantum chaos. **2**, 3146 (2007).

[haa01] F. Haake. *Quantum Signatures of Chaos. 2nd edition.* Springer Berlin (2001).

[hoeh08] R. Höhmann, U. Kuhl, and H.-J. Stöckmann. Scattering fidelity for a local perturbation. *Phys. Rev. Lett.* **100**, 124101 (2008).

[hol86] A. Holle, G. Wiebusch, J. Main, B. Hager, H. Rottke, and K. H. Welge. Diamagnetism of hydrogen atom in the quasi-Landau regime. *Phys. Rev. Lett.* **56**, 2594 (1986).

[jac01] P. Jacquod, P. G. Silvestrov, and C. W. J. Beenakker. Golden rule decay versus Lyapunov decay of the quantum Loschmidt echo. *Phys. Rev. E* **64**, 055203(R) (2001).

[jal01] R. A. Jalabert and H. M. Pastawski. Environment-independent decoherence rate in classically chaotic systems. *Phys. Rev. Lett.* **86**, 2490 (2001).

[koeb10] B. Köber, U. Kuhl, H.-J. Stöckmann, T. Gorin, D. V. Savin, and T. H. Seligman. Microwave fidelity studies by varying antenna coupling. *Phys. Rev. E* **82**, 036207 (2010).

[koeb11] B. Köber, U. Kuhl, H.-J. Stöckmann, A. Goussev, and K. Richter. Fidelity decay for local perturbations: Microwave evidence for oscillating decay exponents. *Phys. Rev. E* **83**, 016214 (2011).

[kuh07] U. Kuhl. Wave functions, nodal domains, flow, and vortices in open microwave systems. *Eur. Phys. J. Special Topics* **145**, 103 (2007).

[lau07] D. Laurent, O. Legrand, P. Sebbah, C. Vanneste, and F. Mortessagne. Localized modes in a finite-size open disordered microwave cavity. *Phys. Rev. Lett.* **99**, 253902 (2007).

[leh55] H. Lehmann, K. Symanzik, and W. Zimmermann. On the formulation of quantized field theories. *Nuov. Cim.* **1**, 205 (1955).

[lob03] O. I. Lobkis and R. L. Weaver. Coda-wave interferometry in finite solids: Recovery of P-to-S conversion rates in an elastodynamic billiard. *Phys. Rev. Lett.* **90**, 254302 (2003).

[lob08] O. I. Lobkis and R. L. Weaver. Scattering fidelity in elastodynamics. ii. further experimental results. *Phys. Rev. E* **78**, 066212 (2008).

[lor63] E. N. Lorenz. Deterministic non-periodic flow. *J. of the Atmospheric Sciences* **20**, 130 (1963).

[los76] J. Loschmidt. Über den Zustand des Wärmegleichgewichtes eines Systems von Körpern mit Rücksicht auf die Schwerkraft. *Sitzungsberichte der Akademie der Wissenschaften, Wien, II* **73**, 128 (1876).

[mah69] C. Mahaux and H. A. Weidenmüller. *Shell-Model Approach to Nuclear Reactions.* North-Holland Amsterdam (1969).

[mai86] J. Main, G. Wiebusch, A. Holle, and K. H. Welge. New quasi-Landau structure of highly excited atoms: The hydrogen atom. *Phys. Rev. Lett.* **57**, 2789 (1986).

[meh63] M. L. Mehta and F. J. Dyson. Statistical theory of the energy levels of complex systems. V. *J. Math. Phys.* **4**, 713 (1963).

[nak06] Shigeru Kanemitsu Mikio Nakahara and Martti M. Salomaa. *Physical Realizations of Quantum Computing: Are the DiVincenzo Criteria Fulfilled in 2004? Osaka, Japan, 7-8May 2004 [With CDROM].* World Scientific Publishing Co Pte Ltd Singapore (2006).

[nie00] M. A. Nielsen and I. L. Chuang. *Quantum Computation and Quantum Information.* University Press Cambridge (2000).

[per00] E. Persson, I. Rotter, H.-J. Stöckmann, and M. Barth. Observation of resonance trapping in an open microwave cavity. *Phys. Rev. Lett.* **85**, 2478 (2000).

[per84] A. Peres. Stability of quantum motion in chaotic and regular systems. *Phys. Rev. A* **30**, 1610 (1984).

[poi08] H. Poincaré. *Science et méthode.* Flammarion Paris (1908).

[poi92] H. Poincaré. *Les Méthodes nouvelles de la Mécanique Célesté.* Gauthier-Villars Paris (1892).

[por65] C. E. Porter. *Statistical Theory of Spectra: Fluctuations.* Academic Press New York (1965).

[sch05a] R. Schäfer, T. Gorin, T. H. Seligman, and H.-J. Stöckmann. Fidelity amplitude of the scattering matrix in microwave cavities. *New J. of Physics* **7**, 152 (2005).

[sch05b] R. Schäfer, H.-J. Stöckmann, T. Gorin, and T. H. Seligman. Experimental verification of fidelity decay: From perturbative to Fermi golden rule regime. *Phys. Rev. Lett.* **95**, 184102 (2005).

[seb90] P. Šeba. Wave chaos in singular quantum billiard. *Phys. Rev. Lett.* **64**, 1855 (1990).

[so95] P. So, S. M. Anlage, E. Ott, and R. N. Oerter. Wave chaos experiments with and without time reversal symmetry: GUE and GOE statistics. *Phys. Rev. Lett.* **74**, 2662 (1995).

[sok89] V. V. Sokolov and V. G. Zelevinsky. Dynamics and statistics of unstable quantum states. *Nucl. Phys. A* **504**, 562 (1989).

[sok92] V. V. Sokolov and V. G. Zelevinsky. Collective dynamics of unstable quantum states. *Ann. Phys. (N.Y.)* **216**, 323 (1992).

[sri91] S. Sridhar. Experimental observation of scarred eigenfunctions of chaotic microwave cavities. *Phys. Rev. Lett.* **67**, 785 (1991).

[ste92] J. Stein and H.-J. Stöckmann. Experimental determination of billiard wave functions. *Phys. Rev. Lett.* **68**, 2867 (1992).

[ste95] J. Stein, H.-J. Stöckmann, and U. Stoffregen. Microwave studies of billiard Green functions and propagators. *Phys. Rev. Lett.* **75**, 53 (1995).

[stoe02] H.-J. Stöckmann, E. Persson, Y.-H. Kim, M. Barth, U. Kuhl, and I. Rotter. Effective Hamiltonian for a microwave billiard with attached waveguide. *Phys. Rev. E* **65**, 066211 (2002).

[stoe10] H.-J. Stöckmann. Microwave billiards and quantum chaos. *Scholarpedia* **5**, 10243 (2010).

[stoe90] H.-J. Stöckmann and J. Stein. "Quantum" chaos in billiards studied by microwave absorption. *Phys. Rev. Lett.* **64**, 2215 (1990).

[stoe99] H.-J. Stöckmann. *Quantum Chaos - An Introduction.* University Press Cambridge (1999).

[str00] R. F. Streater and A. S. Wightman, editors. *PCT, spin and statistics, and all that.* Landmarks in Mathematics and Physics. Princeton Univ. Press Princeton (2000).

[tan07] G. Tanner and Søndergaard. Wave chaos in acoustics and elasticity. *J. Phys. A* **40**, 443(R) (2007).

[usa98] G. Usaj, H. M. Pastawski, and P. R. Levstein. Gaussian to exponential crossover in the attenuation of polarization echoes in NMR. *Mol. Phys.* **95**, 1229 (1998).

[ver85] J. J. M. Verbaarschot, H. A. Weidenmüller, and M. R. Zirnbauer. Grassmann integration in stochastic quantum physics: The case of compound-nucleus scattering. *Phys. Rep.* **129**, 367 (1985).

[wig55] E. P. Wigner. Lower limit for the energy derivative of the scattering phase shift. *Phys. Rev.* **98**, 145 (1955).

Acknowledgements

I thank everybody who contributed to the success of this work:

- My supervisor Prof. Dr. Hans-Jürgen Stöckmann for giving me the opportunity to do my PhD in his group, for good collegial relationship and all valuable help and guidance.
- Prof. Dr. Peter Lenz as the second advisor for his kind interest in this work.
- Prof. Dr. Ulrich Kuhl for fruitful discussions and for all his patience with me. He always supported and encouraged me during my time in the quantum chaos group.
- Sonja Barkhofen, Stefan Gehler, Tobias Weich, Otto Dietz, Kristof Beck, Alexander Potzuweit, Dr. Timur Tudorovskiy and Dr. Ruven Höhmann for a very pleasant (working) atmosphere during my time in the quantum chaos group.
- Prof. Dr. Klaus Richter and Dr. Arseni Goussev for the collaborations on the study of fidelity decay for a pistonlike boundary perturbation.
- Prof. Dr. Thomas Seligman, Prof. Dr. Thomas Gorin and Dr. Dmitry Savin for the collaborations on the study of coupling fidelity.
- The institutes of the faculty of physics, especially the fine mechanical workshop.
- The DFG for financial support via FOR760
- My family and friends, especially my dear Astrid, for listening my problems, caring for distraction and always encouraging me to finish this work.

Wissenschaftlicher Werdegang

2003-2008	Studium der Physik und Mathematik an der Philipps-Universität Marburg
2007	Staatsexamensarbeit: *Fidelity-Untersuchungen an chaotischen Mikrowellenresonatoren* in der AG Quantenchaos (Prof. Stöckmann)
2008	Erstes Staatsexamen für das Lehramt an Gymnasien (Physik und Mathematik)
2008-2011	wissenschaftlicher Mitarbeiter und Promotionsstudent am Fachbereich Physik der Philipps-Universität Marburg in der AG Quantenchaos